# Development of a DNA Assay Based on Digital Quantification of Single Molecules by Total Internal Reflection Fluorescence Microscopy

A senior honors thesis submitted by

Michael M. Lacy

Department of Chemistry

Tufts University

May 2012

Advisor: Professor David R. Walt

**Acknowledgements**

I would like to thank my research advisor Professor David Walt for his guidance and for giving me the opportunity to pursue this research project over the past two years. It has been an invaluable experience and I am grateful for his support. I would also like to thank Professor Joshua Kritzer for serving on my thesis committee as well as his guidance as my academic advisor. I would especially like to thank Dr. Manuel Palacios for his mentoring as a post-doctoral fellow in the Walt group.

I would like to thank the other graduate student and post-doc members of the Walt group who have helped me: Stephanie Schubert for her guidance and help with experiments, preparing some sample surfaces and DNA-QDs for early DNA experiments, Aaron Phillips for his help and insights at the start of the project, Dr. Maël Manesse for his help with microfluidic platforms, and Marcin Rojek and Pratyusha Mogalisetti for their help with enzyme experiments. This project would not have been possible without all of you and I am happy to have been able to work with such a group of scientists. I would also like to thank fellow undergraduates Mitchell Duffy (Tufts 2012), Wojciech Voitek Musiał (MIT 2013) and Constantin Berzan (Tufts 2012) for their help teaching me the computer programming needed to build the image analysis program.

I acknowledge Tufts University, the Office of Undergraduate Education Summer Scholars Grant, and Quanterix Corp. for funding.

# Table of Contents

**Abstract**

Single molecule detection schemes promise the ability to reach the ultimate limit of detection: one molecule. In this project we use Total Internal Reflection Fluorescence Microscopy (TIRFM) to detect individual biomolecules for quantification. TIRFM has the advantage of delivering high contrast images and has become a standard method for the optical detection of single molecules. Here TIRFM is presented as a method to determine the concentration of molecules in solution by correlating digital counts of single fluorescent molecules immobilized on a TIRF probed surface. The luminescent reporters used in this project are quantum dots (QDs), semiconductor nanocrystals known for their remarkable brightness and stability. Despite the numerous outstanding photophysical properties of QDs, observations of single QDs also display a pronounced intermittent fluorescent behavior, posing a challenge for detecting single QDs. This thesis demonstrates a reliable method of detection taking advantage of these fluctuations of the signal. The quantitative methodology developed here for digital quantification of single QDs enables detection at the sub-femtomolar level, and can be applied to biological applications for quantification of low levels of DNA.

# 1. Introduction

## 1.1 Single Molecule Studies

The state of the art in biochemical studies and sensing applications lies at the single molecule level. DNA sequencing, clinical diagnostics, and many other areas can benefit from the application of single molecule detection (SMD) methods. Using various techniques to isolate, visualize, and analyze the behavior of individual biomolecules, recent research has led to a much more detailed understanding of molecular behavior. Direct observation of individual molecules over time can uncover rare molecular events in a population of molecules and avoid the errors and biases that can often occur when observing a bulk sample. Especially important for quantitative biological analyses is that SMD methods promise the possibility of the ultimate limit of detection: one molecule.

Recent studies have demonstrated various advantages of single molecule methods. For example, by isolating individual enzyme molecules and tracking the catalytic activity of each separately, it has been shown that a bulk sample is actually comprised of a population of enzymes with varying individual activities (1). This kind of detailed information is only accessible at the single molecule level, as distributions and sub-populations will simply contribute to a bulk average property. Similarly, highly detailed information about the kinetics of molecular binding events (2-4) and specific mechanisms and molecular interactions (5-6) can be revealed through single molecule studies. The detailed information revealed by single molecule studies is contributing greatly to our understanding of how biological molecules behave.

By similar reasons, studies of single cells can also provide valuable information not accessible at the population level. Cellular processes such as transcription, translation and

acquisition of mutations can vary significantly from cell to cell. For example, transcription requires binding of several specific proteins to DNA sequences and relies on diffusion of all the proper molecules within the cell. The number of events and processes that must work together is impressively large, and small variations in a particular cellular microenvironment can result in significant variations downstream. The stochastic nature of these processes causes gene expression to vary significantly between different cells under the same conditions in a population. Unfortunately, these details are lost in conventional methods that only measure collective responses over an entire population. Recent research has shown that in a population of genetically identical cells, the numbers of both the mRNA transcript and the protein for a given gene can vary widely (7). Likewise, the accumulation of mutations occurs by individual changes in individual cells' genomes. Thus, being able to study each cell on its own can give a much more detailed picture of the locations and effects of each mutation, without being hidden in the population average (8).

Traditionally, detection of small amounts of sample has relied on amplification methods to generate a detectable amount of molecules. For example, the polymerase chain reaction (PCR) uses a DNA polymerase enzyme and specific oligonucleotide primers to create millions of copies of a specific gene sequence (9). PCR can be used as a sample preparation step followed by other detection techniques or it can be performed quantitatively, measuring the amount of DNA or mRNA copied in real time (although this process does not rely on single molecule detection but rather a bulk fluorescence measurement). Another commonly used method is the enzyme-linked immunosorbent assay (ELISA). In this method, the target antigen is captured on a solid support and then its presence is detected by binding of an antibody conjugated to an

enzyme which converts a substrate to a detectable product. Usually carried out in a microtiter plate, the measurement relates the amount of fluorescent product in the well to the amount of target in the original sample (10). In both PCR and ELISA however, the amplification process is not perfect and can introduce errors and biases to the end result. The amplification can be biased by the original ratio of species in the population and can be skewed by high amounts of other interfering species. In addition, proper signal amplification usually requires a sufficiently high number of molecules of the analyte to be amplified accurately for detection (11).

An additional advantage of SMD and single-cell analysis is the decreased sample size. High-throughput techniques can be applied with minimal reagent usage, lowering costs for applications such as gene sequencing and clinical diagnostics. Reducing the amount of cellular sample required can also be significant in clinical settings when a sample might not contain enough cells of interest to be detected by conventional tests or if a large tissue biopsy may be too invasive. With this increased information available from a smaller amount of material, SMD techniques have the potential to vastly improve methods in applications as diverse as DNA sequencing, clinical diagnostics, and basic biochemical research (12, 13, 14).

### 1.2 Digital Quantification of Single Molecules

Many conventional methods for quantitative analysis rely on relating a bulk property to an amount of analyte, as properties such as fluorescence intensity or absorption are proportional to concentration. In addition to the disadvantages described above, this principle is often hampered by the sensitivity, dynamic range and limit of detection of the instrument. In contrast, digital quantification by counting at the single-molecule level accounts for the discrete

nature of a population of molecules rather than having to rely on an indirect measure of some secondary signal or bulk property. This discrete counting is where quantitative SMD has the potential for the ultimate limit of detection and sensitivity.

As SMD methods have seen increasing application over the past twenty years, the focus has been consciously shifting away from the analog nature of conventional methods to the digital nature of single molecules (14, 15, 16). Just as a computer deals with digital bits to store information, we can obtain a digital response from discrete molecules in a sample. While bulk assays can require millions to billions of molecules to produce a detectable signal that must be related to an amount of analyte, digital quantification by SMD obtains a signal from each individual molecule. Although there are practical challenges to achieving accurate measurements at very low levels, many techniques have been demonstrated for SMD of biomolecules.

Various methods have been described to detect signal from individual molecules and maintain the digital nature of a molecular population. One strategy still relies on conventional amplification methods but confines the amplification reactions to a small enough volume or to a small amount of sample that the signal collected can be attributed to the presence of one molecule. Two examples are so-called digital PCR and digital ELISA. By compartmentalizing individual molecules, the amplified product from each molecule of analyte can be counted as a digital signal indicating the presence of a single molecule. While several methods using these principles have been applied to achieve low limits of detection (14, 17, 18), they are still fairly complex, indirect methods. We would like to use methods that allow direct detection of single molecules for counting.

Technological advances have enabled visual detection of single fluorophore molecules. Methods such as confocal microscopy and total internal reflection fluorescence microscopy (TIRFM) are able to visually resolve single molecules and have been used in various studies to detect individually labeled molecules (15,19). Various strategies are used to specifically label biomolecules of interest and detect their presence for quantitative measurements. Other commonly used methods not relying on visual detection include atomic force microscopy and surface plasmon resonance imaging. While each of these techniques has advantages, our project uses TIRFM. We capture specific molecules of interest and observe fluorescence from individual molecules bound by specific binding events.

**1.3 TIRFM Principles and Applications**

Of the various methods used for single molecule visualization, TIRFM has certain advantages that make it particularly suited for our purposes of single molecule quantification. While the phenomenon of total internal reflection was first observed in 1854, it was not applied as a microscopy tool until the 1960's and began to see increased use in biological applications in the 1980's due to improvements in the theoretical understanding of TIRFM and advances in the technological capabilities of fluorescent molecules (20, 21). The apparatus used is similar to other conventional fluorescence microscopy techniques, but differs in the specific arrangement of the optics and mode of sample illumination.

The principle of total internal reflection can be understood through Snell's Law, which describes the refraction of light at the interface of two materials. The angle of refraction ($\theta_2$)

depends upon both the angle of incidence ($\theta_1$) and the refractive index of each material ($n_1$ and $n_2$) according to the equation:

$$n_1 \sin\theta_1 = n_2 \sin\theta_2 \qquad \text{[Eq. 1.1]}$$

The critical angle $\theta_c$ is the angle where the refracted light travels along the interface of the materials, or $\theta_2 = 90^o$. This angle is obtained by substituting and rearranging Eq. 1.1:

$$\theta_c = \sin^{-1}\left(\frac{n_2}{n_1}\right) \qquad \text{[Eq. 1.2]}$$

This process is illustrated in Figure 1.1 below.

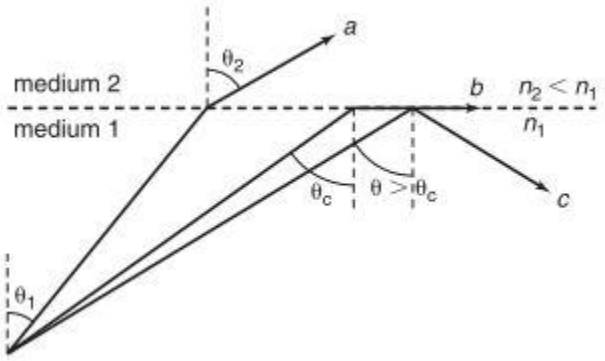


**Figure 1.1: Illustration of refraction and total internal reflection.** For an light ray encountering a boundary between two materials, the resulting angle of refraction ($\theta_2$) is dependent on the incident angle ($\theta_1$) and the refractive indices of the two materials ($n_1$ and $n_2$), as described by Snell's Law. [Image reprinted from(22)]

For an incident angle greater than the critical angle, while the light is totally internally reflected and does not enter the second medium, an evanescent electromagnetic field is established at the interface. This evanescent field propagates into the second medium and decays exponentially such that the intensity at a depth *z* is given by:

$$I = I_o \exp(-z/d) \qquad \text{[Eq. 1.3],}$$

Where $I_o$ is the incident intensity and the characteristic exponential decay depth *d* is given by:

$$d = \frac{\lambda}{4\pi n_2}\left(\frac{\sin^2\theta_1}{\sin^2\theta_c} - 1\right)^{-1/2} \qquad \text{[Eq. 1.4],}$$

For $\lambda$ the wavelength of light and $\theta_1$ (angle of incidence), which is greater than $\theta_c$ (critical angle). The relative intensity at various depths in an aqueous solution above a glass microscope slide can be determined using these equations. For a typical TIRFM setup a molecule situated at 0, 1, 10, 100, or 1000 nm above a surface will experience relative intensities of 1.0, 0.99, 0.92, 0.43, and 0.0002, respectively (21). This phenomenon allows for illumination of fluorescent molecules near the surface with very little illumination into the rest of the sample and thus very low background fluorescence.

Two approaches are commonly used to achieve TIR, which differ in the optical setup for introducing the illumination (Fig. 1.2). In prism-type TIRFM, the illuminating laser is introduced through a prism to hit the sample surface above the critical angle (Fig. 1.2A). More recently, high-numerical aperture (NA) objectives have allowed the laser to be introduced through the objective (Fig. 1.2B). A high-NA objective (usually 1.4 or higher) allows for both high resolution imaging and introduction of the laser through the objective at a sufficiently high angle (greater than the critical angle).

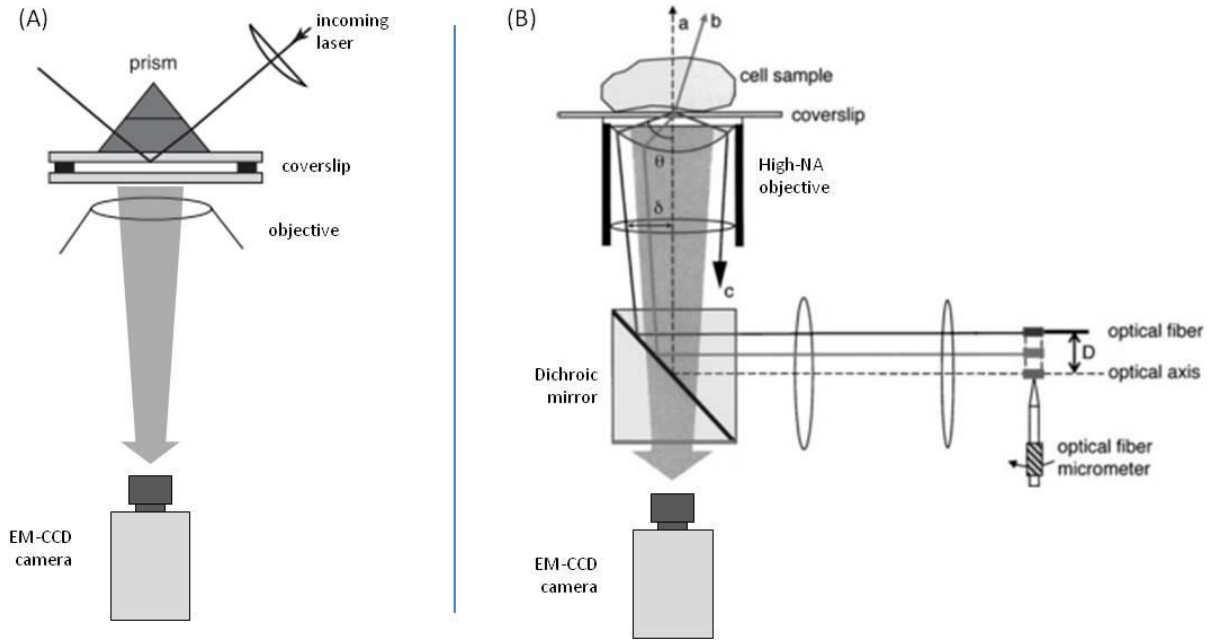


**Figure 1.2: Two schemes for achieving TIRFM**. (A) In prism-type TIRFM, the laser is introduced through a prism to illuminate the sample opposite from the objective. (B) In objective-type TIRFM, the laser is introduced from an optical fiber and passed through a high-NA objective. The incident angle is controlled by positioning the beam away from the center of the optical axis. Additional optics such as mirrors and filters can be used to direct illumination and emission light and select wavelengths. Fluorescence detection can be accomplished using a CCD camera or other detector. [Image adapted from (22)].

As both methods only illuminate a narrow layer near the surface, samples are often prepared by depositing cells or specific molecules on the glass (or quartz) surface for detection (22, 20). There have also been cases where the fluorescently tagged molecules are left free in solution and detected upon diffusion into the illumination layer (23).

TIRFM has been applied in many studies, for both fundamental biochemical research and applied quantitative analyses. The single-molecule resolution achievable by TIRFM has been used in a wide variety of studies. For example, TIRFM has been used to visualize the motion of individual myosin proteins traversing an actin filament (5), to study the physical behavior of individual fluorescent molecules (24, 25), to study RNA folding kinetics (26), and to visualize DNA single-nucleotide polymorphisms (SNPs) (27). In quantitative applications, TIRFM

has been applied to detection of nucleic acids (DNA, RNA) (23, 28, 29, 30), detection of proteins (19) and study of protein-protein interactions (31). TIRFM is a versatile method, and various experimental schemes have been devised to capture and visualize specific molecules in the limited detection volume near or at the surface.

### 1.4 Quantum Dots as Fluorescent Reporters

Fluorescent molecules absorb and emit light at characteristic wavelengths, allowing detection of specific molecules. Dye molecules are often conjugated to specific biomolecules through various chemical means so that the fluorescent probe can act to quantitatively signal the presence of a specific target or interaction. Shown in Figure 1.3 are three common organic dye molecules and their excitation and emission spectra.

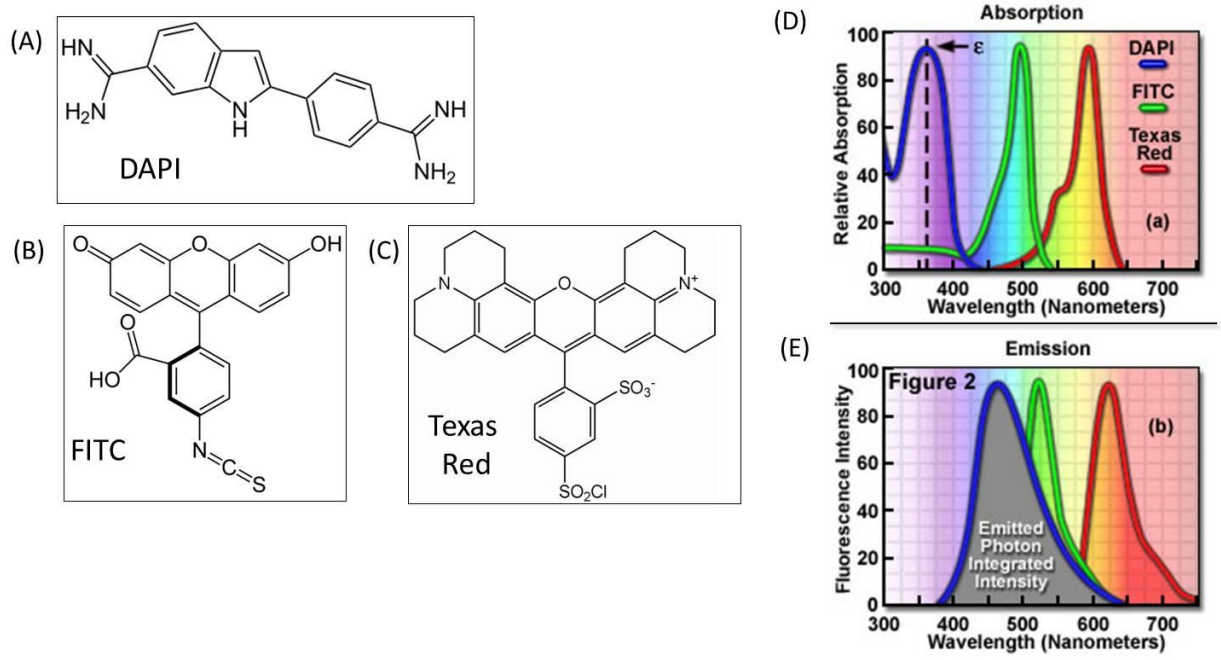


**Figure 1.3: Structures and excitation/emission spectra for three example organic dyes.** (A) 4',6-diamidino-2-phenylindole (DAPI), (B) Fluorescein isothiocyanate (FITC), and (C) Texas Red. (D) and (E) Absorption and emission spectra for these dyes. [Spectra from www.olympusfluoview.com]

The luminescent probes used in this project are quantum dots (QDs), semiconductor nanocrystals known for their remarkable brightness and stability. In contrast to organic dye molecules, QDs have notably different optical properties, providing several advantages for their use as fluorescent probes. Semiconductor materials (such as CdSe, CdTe, ZnS and others) can be crystallized in colloidal form to create nanoparticles (see Figure 1.4). When a particle's size is made small enough to interfere with the quantum mechanical behavior of the material (a few nanometers to tens of nanometers), interesting phenomena can occur. In this case, QDs can undergo fluorescence as a particle behaving like a molecule (32, 33, 34). While conventional fluorescent dyes are usually large organic molecules with aromatic systems that can easily absorb and emit photons of specific wavelength, QDs are larger particles that fluoresce due to quantum mechanical effects of the particle's size on its semiconductor behavior. Several features of QDs make them particularly desirable for use as fluorescent probes, including their tunability, their exceptional brightness and stability, and their broad excitation and narrow emission spectra. QDs can also be easily conjugated to biomolecules due to their multivalency of surface reactive sites.

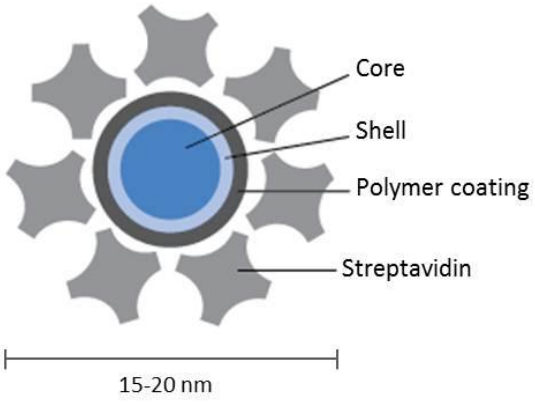


**Figure 1.4: QDot structure.** A schematic of a QDot Streptavidin conjugate, as provided by Invitrogen Corp. [Image adapted from (35).]

Bulk semiconductor materials have electronic energy levels separated into a valence band (occupied) and a conductive band (unoccupied), each a continuum of energy levels. For molecules, the electrons can access discrete orbitals as described by molecular orbital theory, and excitation can cause an electron to transition from the highest occupied molecular orbital (HOMO) to the lowest unoccupied molecular orbital (LUMO). Figure 1.5 illustrates these various electronic configurations and transition behaviors. The electronic configuration of a QD is somewhat intermediate between these two behaviors due to the particle's size (36).

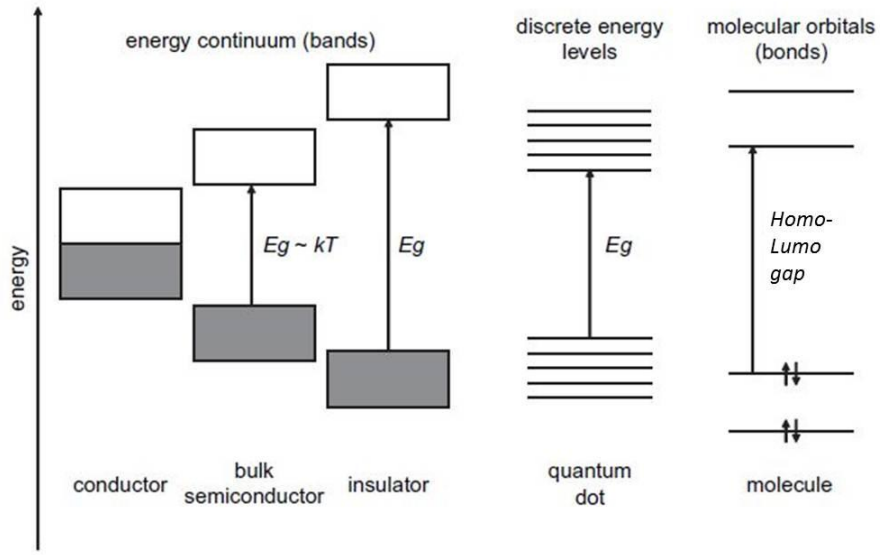


**Figure 1.5: Various configurations of energy levels.** The electronic structure of QDs shares properties of both the energy continuum bands of bulk semiconductors and the discrete nature of molecular orbitals. [Image reprinted from (36)]

Upon absorption of a photon of sufficient energy, an electron is promoted from the valence band to the conduction band, creating a positively charged 'hole'. This electron-hole pair is referred to as an exciton, and the electron and the charge 'hole' interact by Coulombic forces. The physical distance between the electron and the charge 'hole' is described by the Bohr radius of the bulk material and is typically 1 to 10 nm (36). But in a QD, the exciton is confined by the discrete particle's small size and it has been shown that the continuum-like

nature of the valence and conduction bands take on a quantized behavior, with several discrete energy levels behaving similarly to the HOMO-LUMO behavior of molecular orbitals (36). Therefore, the particle can undergo photon absorption and emission very much like a molecule. In addition, the size of the particle (and thus the confinement on the exciton radius) determines the energy gap for the electronic transitions and so the emission wavelength can be engineered during synthesis (see Figure 1.6) (36).

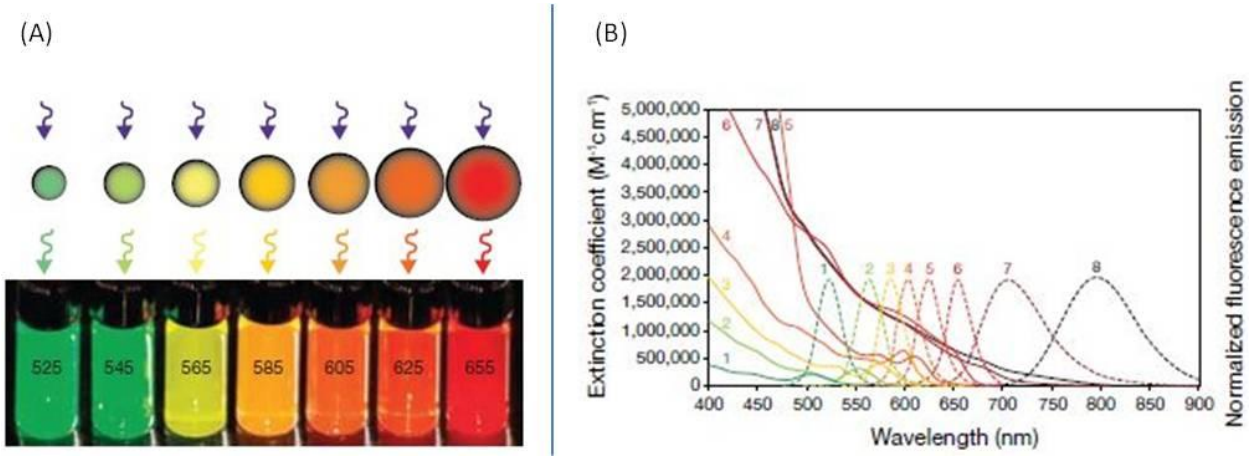


**Figure 1.6: Tunability of QD spectra by size.** (A) Increasing QD particle size yields lower energy band-gap and more red-shifted emission. Wavelengths are shown in nm. (B) Excitation and emission spectra for several commercially available QDs; 1: QDot 525, 2: QDot 565, 3: QDot 585, 4: QDot 605, 5: QDot 625, 6: QDot 705, 7: QDot 800, Invitrogen Corp. [Image reprinted from (35)].

QDs are synthesized by colloidal nanocrystal growth. They can be made of various semiconductor materials, but most commonly include a core of CdSe with a ZnS shell. This core-shell construction enhances the confinement on the exciton and prevents surface reactions and degradation, improving the quantum yield as well as photostability (36). The size of the particle is controlled during synthesis by factors such as temperature, concentration, and duration of the reaction, as well as other chemical components added to the reaction mixture. By stopping the synthesis reaction at a given time, a population of QDs can be created with specific size and emission properties (as in Fig. 1.6).

There has been increasing use over the past fifteen years of QDs in SMD applications, primarily due to their enhanced optical properties and versatility. As techniques for synthesis have improved stability and usability, these advantages over smaller organic dye molecules make single QDs easier to detect. QDs have quantum yields (number of photons emitted per number of photons absorbed) comparable to those of various organic dyes, but their molar absorption coefficient is much higher (10 to 100-fold greater) than most organic dyes (37). A single QD can absorb and emit many photons simultaneously, in contrast to a single organic dye molecule, contributing to a much brighter fluorescence signal. This increased brightness greatly improves the signal/background ratio and makes fluorescence detection much easier for SMD (36, 37). In addition, due to the synthesis process the QD surface is chemically multivalent with a relatively large surface area containing many reaction sites. This feature allows easier, more efficient conjugation to biomolecules, and the possibility of coating a QD particle with many copies of the same biomolecule. This multivalency is an important contrast to organic dye molecules, which usually have one reactive site per dye molecule. With this restriction, a single biomolecule might be conjugated to many dye molecules. But, having more dye molecules conjugated to the same target molecule does not necessarily improve performance - fluorescence can be quenched due to electrostatic interactions and overcrowding effects, and the biomolecule's function may be hindered - and this approach still does not match the fluorescence performance of QDs (37).

The other considerable advantage of QDs over organic dyes is their long photostability. The process of fluorescence involves promoting an electron to a high-energy state and several processes can then occur, only one of which will lead to emission of a photon (fluorescence).

Otherwise, the energy may contribute to a chemical reaction or loss of the electron to the surroundings (ionization), the energy may be dissipated as heat, or the molecule can be trapped in a non-fluorescent triplet state (known as quenching). The degradation of a fluorophore by photochemical reactions, often involving photooxidation, is termed photobleaching, and is an irreversible process. Whereas organic fluorophores usually photobleach after a short period of continuous excitation/emission (few seconds), QDs are capable of continued illumination and fluorescence for comparably very long time scales (many minutes) before photobleaching (37). This photostability makes QDs highly desirable for long time-span experiments as well as making them much easier to work with, eliminating the need for oxygen scavenger systems often used with organic dyes.

Another particularly important feature about QDs' behavior is the shape of their excitation and emission spectra. Due to the unique fluorescence mechanism, QDs of a given size exhibit broad excitation spectra and very narrow emission spectra (Figure 1.6). As mentioned above, the emission spectrum is easily tunable during synthesis of a batch of one particular species of QDs, while the excitation spectrum is less affected. An important result of this feature is that it allows for simultaneous excitation of multiple different species of QDs because their excitation spectra overlap widely. This feature enables multiplexing, tagging different specific biomolecules with different colored QDs that are all excited by one wavelength of illumination. The different emissions can be spectrally separated to detect multiple different targets in parallel (37).

A noted disadvantage of using QDs for SMD is that they fluoresce only intermittently in a process known as 'blinking'. QDs exhibit this unusual blinking behavior by switching between

'on' and 'off' states of emission. The blinking process is stochastic, and can occur anywhere on the timescale of milliseconds to many seconds (36, 38). The physical basis of this behavior is unknown, though it may be due to charge separation and loss of the excited electron to the solution either through reactions on the QD shell surface or by quantum tunneling through the shell layer (36). Blinking can cause difficulty for SMD because in any given observation time one cannot be sure that all the reporters are producing signal. Fluorescence microscopy experiments usually occur on the timescale of several milliseconds of exposure (to minimize photobleaching). If the same observation timescale is used for a sample of QDs, only a fraction will be producing signal. Therefore, different approaches must be used for reliably detecting single QDs.

One method commonly used to overcome this challenge is to simply use a longer observation time. By extending this window of time, one can increase the probability that the QDs will be detected in the 'on' state. Researchers often use this longer observation time and then integrate the signal to improve the detection efficiency in a population of QDs with different blinking behavior (28, 36). Unfortunately this method is not a fully effective solution. Because the behavior of each QD molecule in a sample can be slightly different, the result of integrating each molecule's signal over time will still give a wide distribution of intensities due to the population distribution of different blinking behaviors, and it can still be difficult to separate all QDs from background. This issue is not trivial because the nature of the signal must be thoroughly considered to ensure accurate detection of QDs. In this project, we use a method based on detecting the *fluctuations* of intensity characteristic of a blinking QD. Rather than simply relying on overall signal, we track the intensity over a longer observation time (~15

seconds) and assess the standard deviation of the intensity over time. This method allows us to capture the wide range of blinking behaviors present in a QD population and improves detection efficiency. We demonstrate that the increased signal-to-background ratio improves quantification methods and yields higher sensitivity and a lower limit of detection.

## 2. Methods I: Detection of Single Quantum Dots on TIRFM Platform

### 2.1 Overview

The objective of this study was to develop protocols that will allow for the robust detection of single molecule fluorescence with a high signal-to-noise ratio (SNR) and low non-specific-binding (NSB). Towards this end, various platforms were studied with different experimental considerations. First, experiments were focused on developing methods to immobilize and detect individual quantum dots with a high SNR using TIRFM for single molecule detection. In this chapter, various platform designs and surface functionalization methods that were tried and improved upon are described. Protocols were based on published literature as well as previous work by lab members.

The general strategy was to take advantage of the very strong affinity of the protein streptavidin for the small molecule biotin (reported $K_a$ values range from ~$10^{11}$ to $10^{15}$ $M^{-1}$), commonly used in biochemical detection schemes (2, 39). Streptavidin-conjugated quantum dots (SA-QDs) are captured at the sample surface by binding to biotin that had been covalently attached to the glass microscope slide surface, followed by TIRF microscopy detection.

Initial experiments used biotinylated bovine serum albumin (biotin-BSA) to coat the glass substrate, followed by addition of SA-QDs. This method was simple and easy to perform, and provided many samples for initial understanding of single QD signaling and detection. But, it proved to be inconsistent and was replaced by a more robust method of poly-(ethylene glycol) (PEG) surface functionalization. Briefly, the glass surface is modified with an amino-silane followed by addition of a biotin-PEG-succinimidyl valerate (biotin-PEG-SVA), an amine-reactive ester forming a stable amide linkage at the surface. An important advantage here is

that the PEG surface is known to reduce nonspecific protein adsorption (40, 41). An additional surface preparation method utilized later uses a biotin-PEG-silane reagent, allowing a one-step functionalization. Also, several kinds of designs of silicone and PDMS wells and glass-bottom multi-well plates were tested for these various sample preparation methods. The general scheme is shown in Figure 2.1, as creation of a PEG monolayer with biotin sites scattered on the surface will allow specific SA-QD capture.

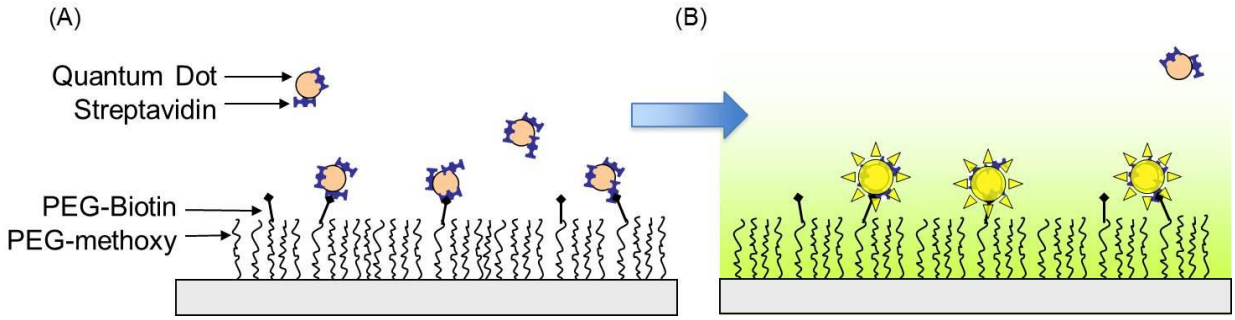


**Figure 2.1: PEG-biotin + Streptavidin-QDot scheme.** SA-QDs in solution will bind to biotin on the PEG monolayer (A). TIRFM enables detection of QDs bound at the surface (B). Note that while some QDs remain in solution (remaining after wash, or due to streptavidin/biotin unbinding), these QDs will be excluded from the excitation and observation volume.

Original PEGylation and silanization protocols were derived from Roy and Ha's published protocols and guides to single molecule experiments (41, 42).

## 2.2 Materials and methods

### *2.2.1 PEG-SVA Functionalization on Amino-silanized Glass in PDMS Wells*

The basic platform consisted of making wells out of a poly-dimethylsiloxane (PDMS) block fixed on a glass coverslip. Glass coverslips (No. 1.5 24 x 40mm, Fisher Scientific #12-544-C, glass thickness 0.16-0.19 mm) can be cleaned and functionalized separately and PDMS blocks with wells cut out can be fixed individually. All reagents were purchased from Sigma-Aldrich at

molecular biology grade unless otherwise specified. QDot 585 Streptavidin Conjugate was purchased from Invitrogen Corp (catalog number Q10111MP). PEG reagents were purchased from Laysan Bio, Inc.

Coverslips were cleaned by successive sonication in a glass staining dish for 20 minutes in 10% Alconox suspension, 5 minutes in Milli-Q ultrapure water, 10 minutes in acetone, 15 minutes in 1M KOH, 10 minutes in Milli-Q water. Cleaned slides were stored in Milli-Q water until use. Silanization with 3-aminopropyl triethoxysilane (APTES) was carried out in a plastic staining dish with a mixture of 50 mL methanol, 2.5 mL acetic acid, and 0.5 mL APTES for 20 minutes, with sonication for one minute after the reaction had proceeded for ten minutes.

PDMS was prepared by 10:1 mixture of Sylgard 184 elastomer base and curing agent (Dow Corning Corp.), centrifuged at 1860*g* for 2 minutes to remove bubbles, poured onto a flat petri dish, degassed under vacuum for 30 minutes and cured at 80$^{O}$C for 1 hour. Holes for the wells were cut using a hole-punch, creating two 7mm-diamater holes in a piece of PDMS polymer. The PDMS pieces were exposed to air plasma treatment for 1 minute and immediately pressed onto cleaned, silanized, and dried coverslips to bond. A schematic of this assembly is shown in Figure 2.2. Wells produced in this way have a base surface area of 38.5 mm$^2$ and hold approximately 100 µL, though the well volume can vary; the thickness of the PDMS layer is determined by the amount of polymer poured into the petri dish before curing.

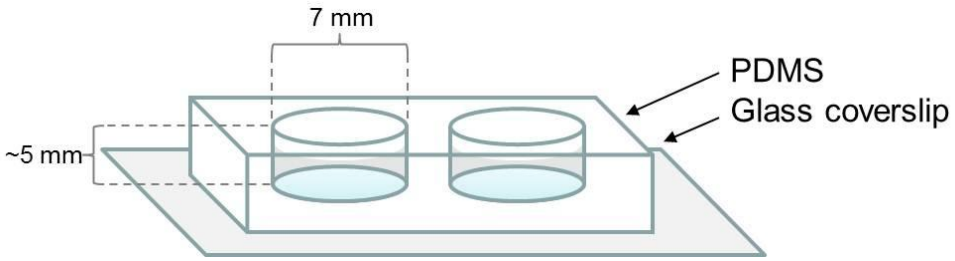


**Figure 2.2: PDMS wells on glass coverslip for PEG-biotin functionalization for SA-QD immobilization.** Glass coverslips are cleaned and silanized before affixing PDMS wells. PEGylation and subsequent SA-QD binding is carried out in wells.

For these experiments, the poly-(ethylene glycol) (PEG) surface was deposited by PEG modified with succinimidyl valerate ester (PEG-SVA). The reaction chemistry scheme is depicted in Figure 2.3 below. The reaction mixture was prepared in a 40:1 ratio of methoxy-PEG-SVA and biotin-PEG-SVA, using 12.5 mg mPEG-SVA (MW 5000) and 0.31 mg biotin-PEG-SVA (MW 5000) per 100 µL of 0.1 M $NaHCO_3$ solution (pH 8.25) (concentrations 250 µM mPEG-SVA and 6.2 µM biotin-PEG-SVA). The solution was mixed thoroughly and centrifuged at 7200*g* for 1 minute to remove bubbles. 40 µL of this mixture was added to each well and allowed to react overnight in a dark, humid chamber.

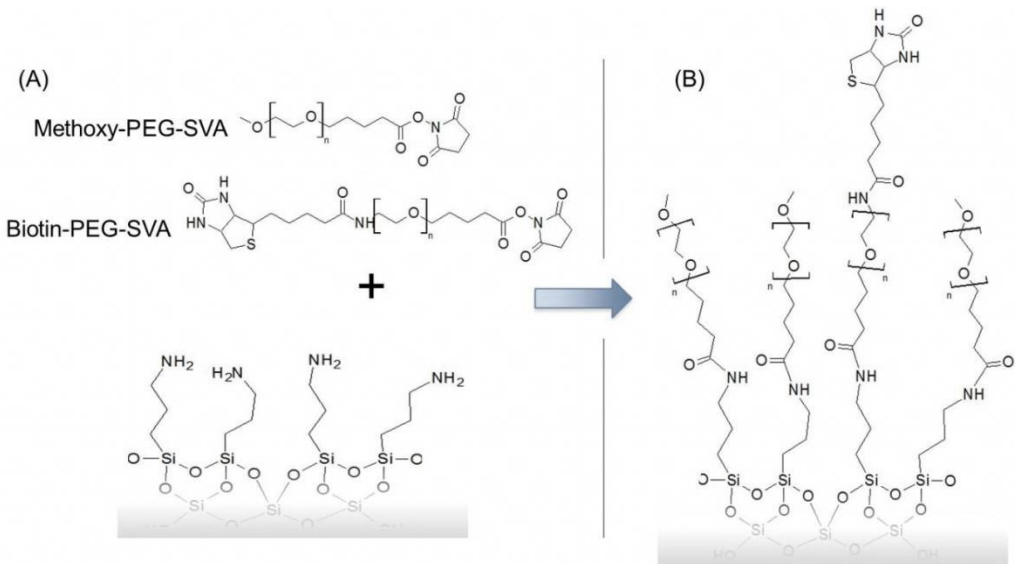


**Figure 2.3: Surface chemistry scheme.** PEG-SVA reagents react with amine groups on glass (A), producing amide linkages (B) with biotin groups scattered on surface. For PEG MW 5000 g/mol, average length n = 114.

After this reaction, wells were washed by immersing in Milli-Q water. Surfaces were blocked by treating with 40 µL of BSA blocking solution (1% BSA in PBS, Thermo Fisher Scientific Inc.) for 1 hour. This solution was removed and 40 µL of streptavidin-conjugated QD (SA-QD) solution (prepared at various dilutions in PBS with 1% BSA) was added to each well and allowed 15 minutes for surface binding. The SA-QD solution was removed and wells were washed three times by removing and refilling with 40 µL borate buffer (Thermo Fisher Scientific, contains 50 mM borate, pH 8.5) and then filled with borate buffer for imaging.

Samples were imaged using a Hamamatsu ImagEM EM-CCD camera on an Olympus IX-71 microscope configured for TIRF microscopy. The field of view with this configuration is 135 µm by 135 µm. Illumination source was a Melles Griot 561 nm diode-pumped solid-state laser, introduced through an Olympus APON 60xO TIRF objective (1.49 NA) with appropriate filter sets for the illumination and emission wavelengths. Images were recorded as 500 frame movies, at 32 frames/sec (approximately 15 sec total observation time) with sensitivity gain 180. QD signaling and detection will be described in Ch. 3, and image analysis for particle counting will be described in Ch. 4.

### *2.2.2 PEG-Silane for One-step Functionalization in Multi-well Plates*

We also developed methods on 384-well glass-bottom plates (glass thickness 0.17 mm, Matrical Bioscience, MGB101-1-2-LG). The same surface preparation methods described earlier can be used in this platform (via pipetting instead of immersion in staining dishes), with slight adjustments. The plastic and glue used for the plates is compatible with all the same reagents except for acetone, which was replaced with isopropanol. Additionally the concentration of

Alconox detergent for cleaning was lowered in order to have a more easily pipette-able solution. The same silanization and PEGylation reaction chemistries can be used, though the surfaces cannot be easily dried in $N_2$, plasma treated, or baked at high temperatures. A one-step functionalization procedure was also developed instead of the separate silanization and PEGylation reactions. For these experiments, PEG deposition was achieved by one reaction with Biotin-PEG-ethoxysilane (MW 3400) and mPEG-ethoxysilane (MW 2000).

Wells were cleaned by filling, mixing and removing solutions via pipette: 100 µL of ultrapure water (Sigma), 100 µL of 5% Alconox solution (washed three times with water after), isopropanol, 50 µL of 1M KOH for 10 minutes, and 100 µL of ultrapure water. The biotin-PEG-silane solution was prepared by dissolving 25 mg biotin-PEG-Silane in 25 mL methanol/1.25 mL acetic acid (final concentration 280 µM). Blank surfaces were prepared by reaction with a solution of 15 mg mPEG-Silane in 25 mL methanol/1.25 mL (final concentration 286 µM). Cleaned wells were rinsed with methanol and 100 µL of the appropriate PEG-silane solution was added to each well. After 2 hours of reaction the wells were rinsed with methanol followed by rinsing with ultra-pure water (Sigma). Wells were either used immediately or filled with ultra-pure water and stored overnight at $4^{o}$C.

Well surfaces were blocked by adding 100 µL of 1% BSA (in 1x PBS) for 1 hour. SA-QD dilutions were prepared in 1% BSA blocking solution at various concentrations. 100 µL of SA-QD solution was added to each well and allowed to bind for 30 minutes before washing three times with 100 µL of 1x PBS buffer. Wells were refilled with PBS buffer for imaging. Imaging conditions are the same as described above, except these experiments used a new laser, Coherent CUBE 488 nm solid-state diode laser, also directed through the objective for TIRF

imaging. This new laser was capable of higher power illumination than the 561 nm laser used previously, and the lower wavelength provides better absorption by the QDs (see spectra given in Fig 1.6).

## 2.3 Results and Discussion

### *2.3.1 Calibration of SA-QDs on Biotin-PEG-SVA Functionalized Surfaces in PDMS Wells*

At first these experiments were carried out to get an initial assessment of the techniques as well as the detection capabilities of the system. By adding solutions of varying SA-QD concentrations to biotin-functionalized wells, the number of QDs counted on the surface can be shown to correlate with concentration. Calibration curves based on the PEG-SVA sample preparation method are shown in Figure 2.4. The data show a dynamic range from $10^{-15}$ M to $10^{-11}$ M, with a limit of detection at approximately 1 fM. Nonlinearity may be due to a variety of factors including saturation of biotin sites, contributions from nonspecific binding of SA-QDs on the surface, or results of the streptavidin-biotin unbinding kinetics over the timescale of the experiments. After the SA-QDs have bound to the surface-immobilized biotin and the solution replaced with buffer, the reversible noncovalent binding will result in some SA-QDs unbinding and being released into solution. When many samples were prepared at once the time between imaging different samples could allow for some unbinding, resulting in fewer QDs detected on the surface.

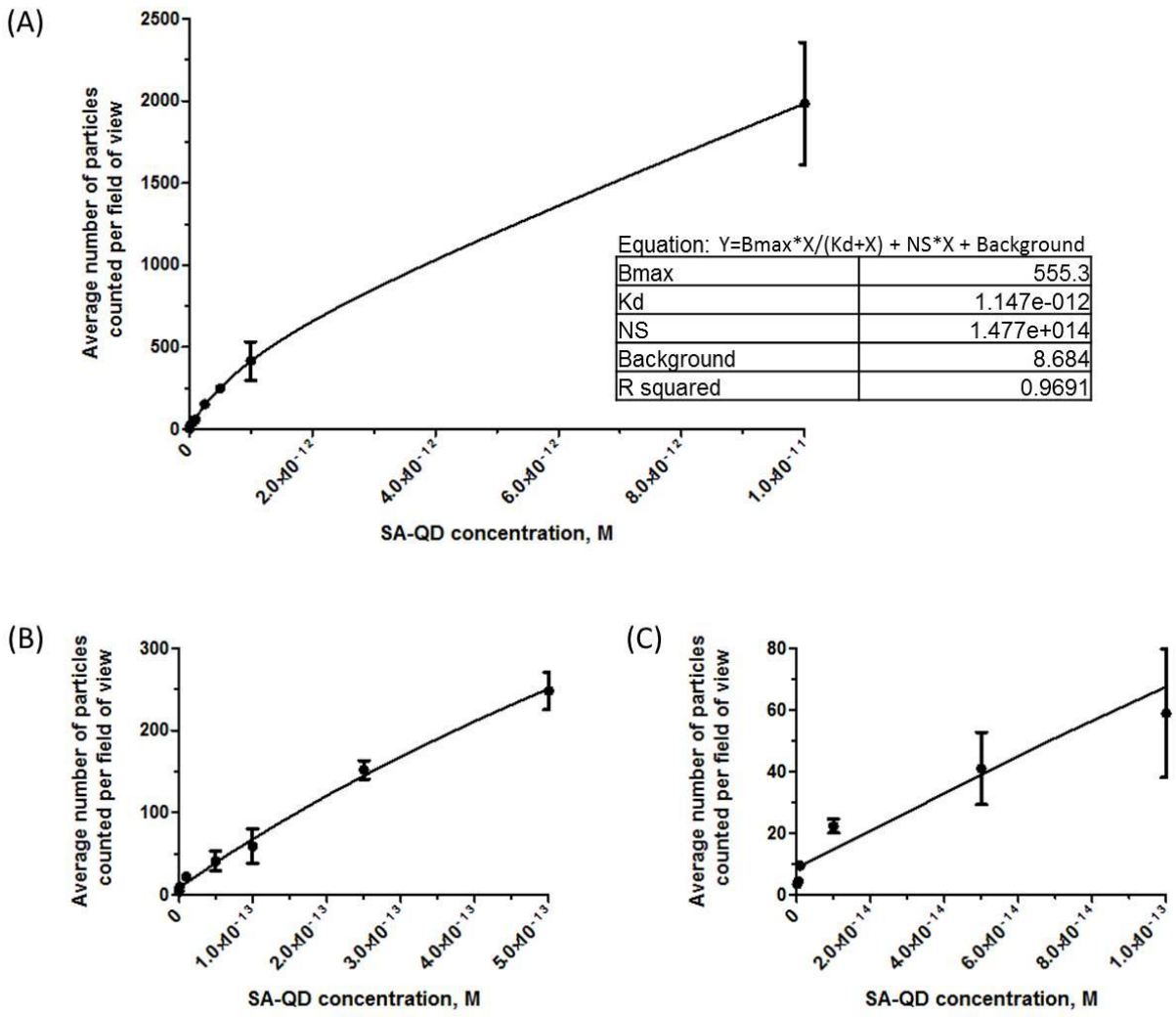


**Figure 2.4: Calibration of QD count vs. concentration on biotin-PEG-SVA functionalized surfaces prepared in PDMS wells.** The data fit with a nonlinear saturation binding curve (A), with values for the equation given in the table. The low concentration range (≤500 fM) is shown in (B), and the very low limit of concentration (≤100 fM) in (C). Error bars are standard deviation of the average of three samples (with 14 images in each sample). Data points are given at concentrations 10 pM, 1 pM, 500 fM, 250 fM, 100 fM, 50 fM, 10 fM, 1 fM, 0.5 fM, 0.25 fM SA-QDs.

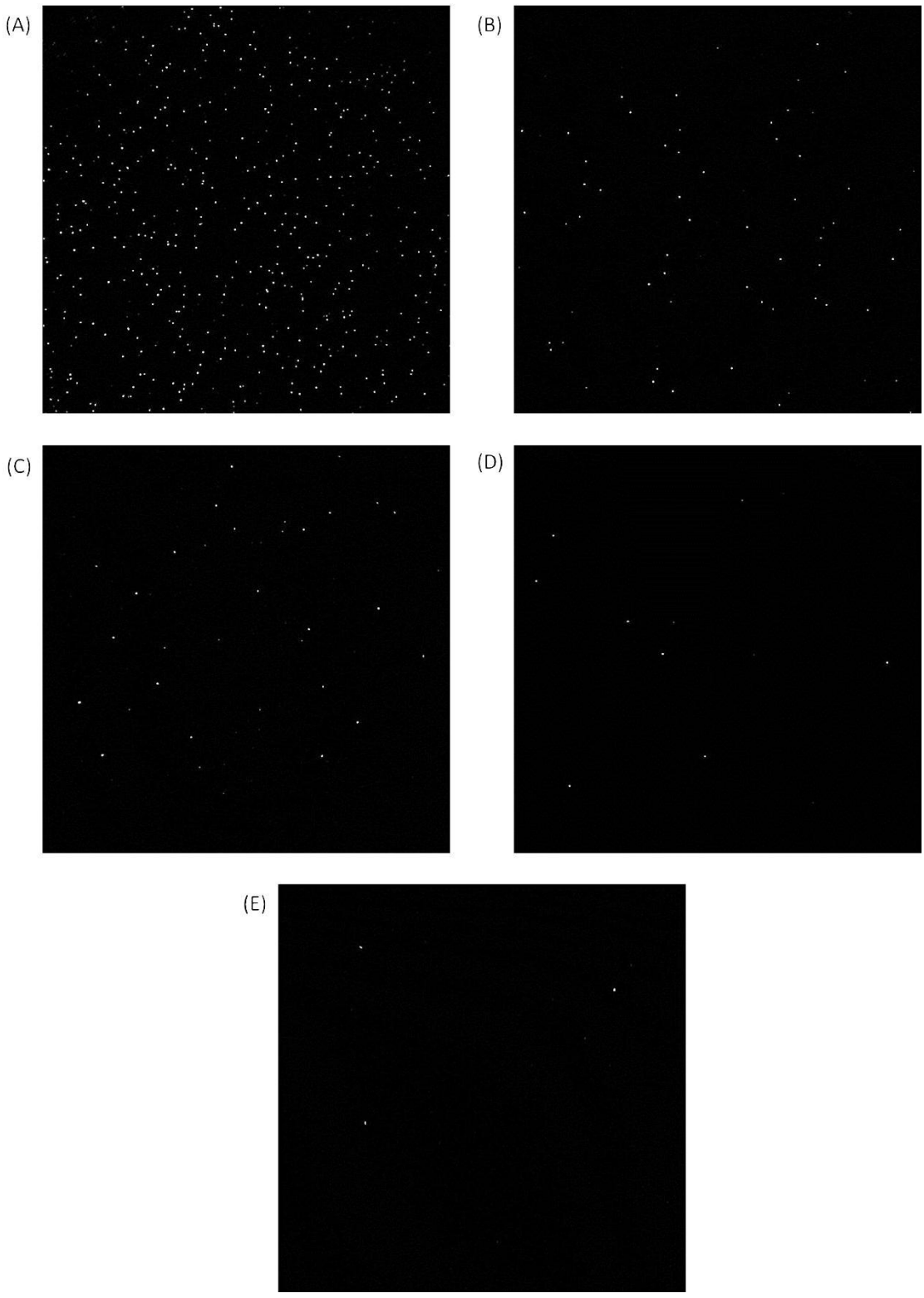


**Figure 2.5: Typical TIRFM images of SA-QDs on biotin-PEG functionalized surfaces at various concentrations.** (A): 1 pM SA-QDs, 524 particles counted; (B): 100 fM, 67 s; (C): 10 fM, 29 counts; (D): 1 fM, 13 counts; (E): 250 aM, 3 counts. Each image is the full field of view 136 µm across, the composite stack projection created as described in Ch. 4.

*2.3.2 Calibration of SA-QDs on Biotin-PEG-Silane Functionalized Surfaces in Multi-well Plates*

Another calibration curve was constructed, demonstrating the capability of the platform using this different surface functionalization method. The calibration curve in Figure 2.6 shows a dynamic range from $10^{-15}$ M to $5*10^{-13}$ M, with a limit of detection at approximately 1 fM.

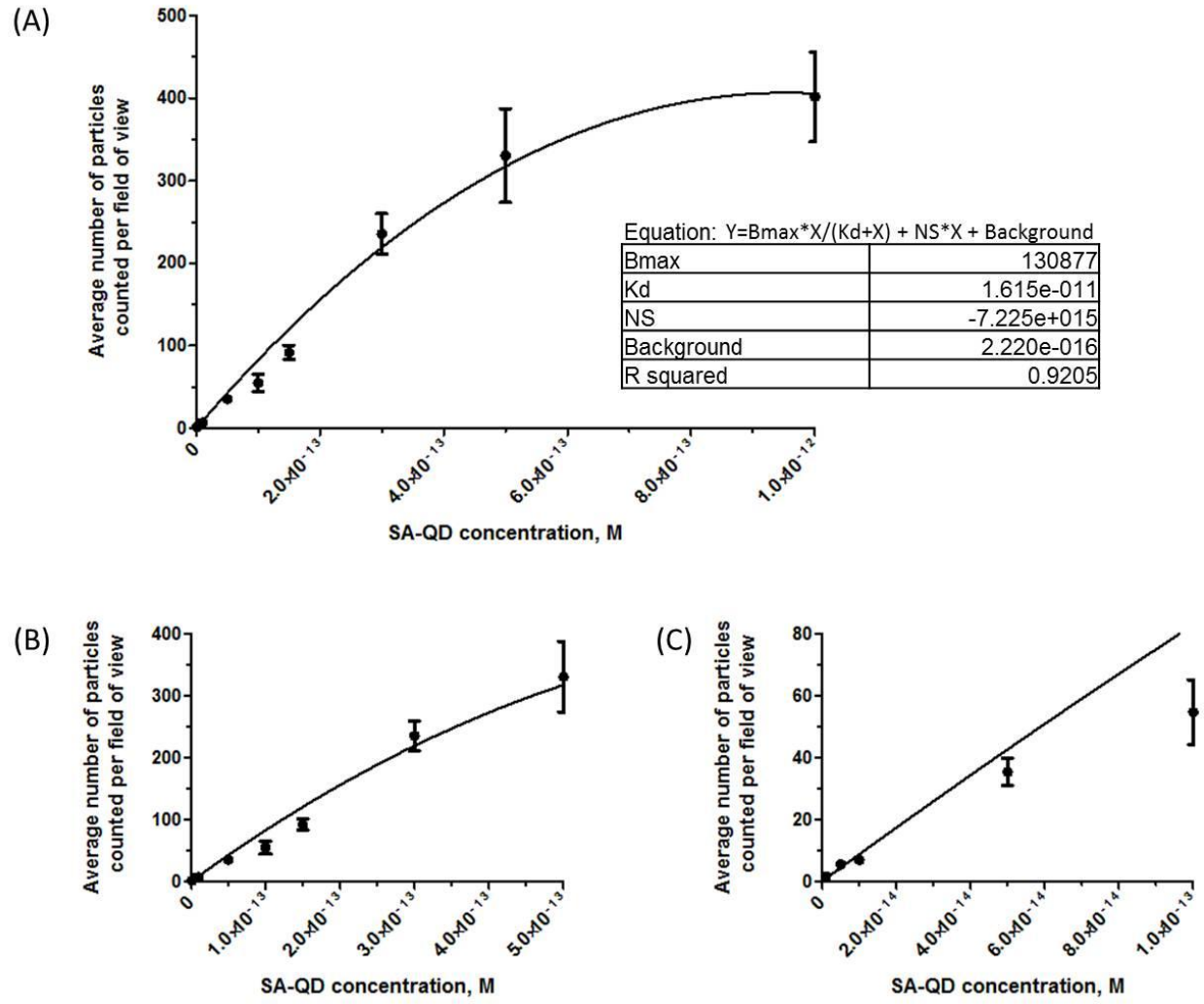


**Figure 2.6: Calibration of QD count vs. concentration on biotin-PEG-silane surfaces prepared in multi-well plates.** The data fit with a nonlinear saturation binding curve (A), with values for the equation given in the table. The low concentration range (≤500 fM) is shown in (B), and the very low limit of concentration (≤100 fM) in (C). Error bars are standard deviation of the average of at least three samples (with 8 images in each sample). Data points are given at concentrations 1 pM, 500 fM, 300 fM, 150 fM, 100 fM, 50 fM, 10 fM, 5 fM, 1 fM SA-QDs.

For these experiments, many samples could be prepared in parallel using the multi-well plates, allowing for better control over the experimental conditions between samples. Additional controls were measured, with samples containing only methoxy-PEG-Silane acting as blanks. Shown below in Figure 2.7 are the same data as above but including the blank sample measurements for each SA-QD concentration.

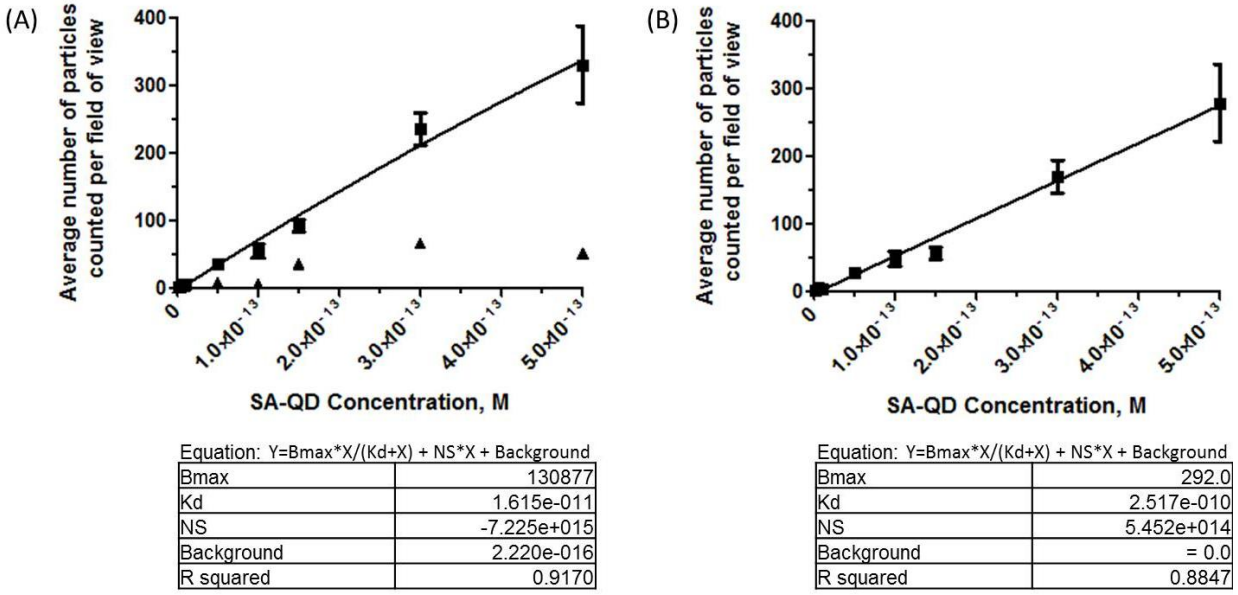


Equation: Y=Bmax*X/(Kd+X) + NS*X + Background

| | |
|---|---|
| Bmax | 130877 |
| Kd | 1.615e-011 |
| NS | -7.225e+015 |
| Background | 2.220e-016 |
| R squared | 0.9170 |

Equation: Y=Bmax*X/(Kd+X) + NS*X + Background

| | |
|---|---|
| Bmax | 292.0 |
| Kd | 2.517e-010 |
| NS | 5.452e+014 |
| Background | = 0.0 |
| R squared | 0.8847 |

**Figure 2.7: Average count vs. SA-QD concentration for biotin-PEG-Silane surfaces with blank mPEG-Silane surfaces.** (A) Counts for samples with Biotin-PEG surfaces (squares) as well as methoxy-PEG surfaces as negative controls (triangles), for SA-QD concentrations 500 fM, 300 fM, 150 fM, 100 fM, 50 fM, 10 fM, 5 fM, 1 fM. The blank-subtracted curve is given in (B), showing a nearly linear trend. Both sets of points are fit with the nonlinear saturation binding curve, with values for the equation given in the tables below.

Unlike the previous experiments with PEG-SVA chemistry, the data here appear to follow a nearly linear relationship in the low limit of concentration (< 500 fM, Fig 2.7B). We believe the origin of the better linear behavior and repeatability might be due to the fact that we are carrying out the experiments in parallel, ensuring equal conditions and better control over the functionalization and incubation protocols, although we do not have a direct proof that this fact is the sole reason for the different behavior. One important difference between

these and earlier preparations was that for the PEG-Silane samples the biotin-PEG was not diluted by methoxy-PEG groups. This choice was made in order to enhance the surface density of biotin sites for increased SA-QD binding and detection. The results here do not indicate an improved limit of detection resulting from this change. Perhaps the greater number of binding sites may be contributing to the difference in linearity. Measurements of these non-biotinylated surfaces suggest that non-specific binding was important in the earlier results as well, likely contributing to the observed deviations from linear behavior. It is important to consider how the nonspecific binding increases with SA-QD concentration, as this will contribute to the background in later DNA assays using SA-QD reporters.

*2.3.3 Biotin-PEG surface and effects on SA-QD binding*

It is difficult to predict what the binding density should be based on the PEG surface. Monolayers of PEG have been studied and used extensively for their ability to decrease protein nonspecific adsorption to glass; however, the surface can be difficult to describe at the molecular level. Monolayers of short PEG chains (MW ~1000 and lower) have been shown to form a brush-like surface, while longer PEG chains can behave differently. Several studies suggest that long PEG chains (MW ~5000) form a highly tangled, intertwined layer. This so-called 'mushroom' layer results in a smoother surface with even less protein adsorption than the 'brush' created by shorter PEGs, but is less uniform and is less dense (40). The flexibility of the PEG chains and their hydrated behavior result in a sparser coverage. The surface would not only be composed of the ends of the PEG chains but also significant portions of the chain itself.

We can estimate the maximum coverage of SA-QDs using the Langmuir adsorption isotherm (43). If we assume complete reaction between the PEG-SVA and amine groups on the surface, the number of binding sites is determined by the surface density of PEG chains contining biotin. Estimating the density of biotin binding sites is difficult in monolayers of high molecular weight PEGs, due to the effects described above. Taking the average footprint area of a solvated PEG chain to be 4.8 $nm^2$ (44) and the surface area of the field of view to be $1.82*10^{-8}$ $m^2$, there are approximately $3.9*10^9$ PEG molecules on the observed surface. At the 1:40 dilution with methoxy-PEG molecules, this gives $9.5*10^7$ biotin sites. For biotin-PEG-silane surfaces prepared with 100% biotin-PEG, all $3.9*10^9$ PEG molecules would have biotin. The Langmuir adsorption isotherm gives the equilibrium fraction of occupied binding sites $\theta_{eq}$ as:

$$\theta_{eq} = \frac{K_a[S]}{1+K_a[S]} \qquad \text{[Eq 2.1].}$$

At a concentration of 1 fM ($10^{-15}$ M) of streptavidin-QDs and using the affinity constant of $K_a \sim 10^{11}$ $M^{-1}$ (2), Equation 2.1 becomes:

$$\theta_{eq} = \frac{10^{11}\,M^{-1}[10^{-15}\,M]}{1+10^{11}\,M^{-1}[10^{-15}\,M]} = \frac{10^{-4}}{1+10^{-4}} = 10^{-4} \text{ occupied biotin/total biotin sites}$$

Using this fraction of binding site occupancy, the number of bound QDs would be $9.5*10^7$ x $10^{-4}$ = 9500 QDs per field of view. This is clearly much higher than the observed number of counts; however, we should account for the fact that the biotin-streptavidin binding is not approaching equilibrium in the timescale of this experiment. We can estimate that perhaps 10% (or less) of the possible binding sites would be occupied after only 15 minutes for 1 fM streptavidin (based on single molecule biotin-avidin kinetic experiments, (2), though the binding kinetics in our experiments are likely further hindered by the conjugation of streptavidin molecules to the relatively large QDs.

Some additional effects may be causing decreased binding. Due to the tangled 'mushroom' structure of the PEGs, a significant portion of biotin molecules might be obscured in the monolayer. Also, it is possible that nonspecific binding of SA-QDs on the side walls of the wells may be decreasing the effective concentration at the surface. We do not have a good way to characterize the effects of these losses. Even with these considerations, this calculated value is clearly much higher than the observed number of about 10 QDs per field of view at the concentration 10 fM. Also it should be noted that these estimates are based on a simplified model and we do not have an accurate measure of the streptavidin binding affinity (which is likely lowered by the QD conjugation) or the PEG surface (which may be more or less dense than surfaces in the reported studies).

Biotin-neutravidin binding kinetics studies suggest that the timescale used in these experiments does not allow equilibrium to be achieved (2). Allowing more time for the SA-QD binding would increase the number of bound QDs but would also increase nonspecific binding; although nonspecific binding will follow different kinetic behavior, it will generally increase with higher SA-QD concentration and longer binding time. Another important consideration is the unbinding kinetics. Wayment and Harris prepared biotin-functionalized surfaces and allowed a 13.3 pM solution of tetramethylrhodamine-labeled neutravidin to accumulate on a biotin-functionalized surface for one hour to reach equilibrium saturation of the biotin sites and then monitored decrease in bound neutravidin over several hours. Their results indicate that after 1 hour approximately 75% of the immobilized neutravidin has become unbound from the initially fully saturated surface (2). Although our experiments do not reach complete saturation of the available biotin sites, there will still be some unbinding when the SA-QD solution is removed

and replaced with buffer. This suggests that our measurements may be compromised by the time necessary to image all the samples, during which dissociation may occur. When many samples were prepared in parallel to be measured in one experiment, they were staggered in time to ensure a similar amount of time between QD binding, removal of QD solution, and imaging.

Later, it was determined that the PEG-SVA reagents do not require an overnight reaction. The PEG-SVA compound has a hydrolysis half-life of 33 minutes in aqueous solution at pH 8 (57). The above procedure for depositing PEG-SVA compounds onto an amine-functionalized surface was modified to use two successive one-hour reactions. The same PEG-SVA reaction mixture is prepared and added to wells for 1 hour, and then is replaced with a second, freshly prepared reaction mixture. The results here for the biotin-PEG-SVA chemistry in PDMS wells were obtained using the original procedure with an overnight reaction. For later experiments using PEG-SVA reagents the protocol was adjusted to use this shortened procedure.

# 3. Quantum Dot Blinking and Detection

## 3.1 Overview

While QDs have noted advantages for single molecule applications, their intermittent blinking poses a practical challenge. Several studies have attempted to characterize QD blinking in order to understand the statistics of the signal as well as the photophysical basis for the phenomenon (36, 45, 46). Researchers attempting to use QDs in single-molecule detection schemes rely on various methods to improve detection of this fluctuating signal such as by increasing the time for signal integration (28, 47), or attempting to decrease the blinking behavior through additives or by engineering novel shell constructions (48, 49). The method of detection demonstrated in this project takes advantage of this fluctuation over time as a means for detection. We demonstrate that the standard deviation of the signal provides a more effective means of distinguishing the QD signal than simple integration.

## 3.2 QD Blinking Behavior

Blinking statistics have been extensively studied since QDs were first observed at the single-molecule scale (36, 38), though the physical basis for the phenomenon is not fully understood. The blinking is known to be stochastic and the probability distributions of on- and off-times have been shown to obey an inverse power law (45, 46). As mentioned in Ch. 1, a common interpretation is that loss of the excited electron leaves the QD trapped in a non-emissive state. Fluorescence is recovered if the escaped electron is recaptured. The stochastic nature of these transitions results in on- and off-times that can vary widely. Figure 3.1 shows time traces typical of the observed fluorescence signal of single QDs.

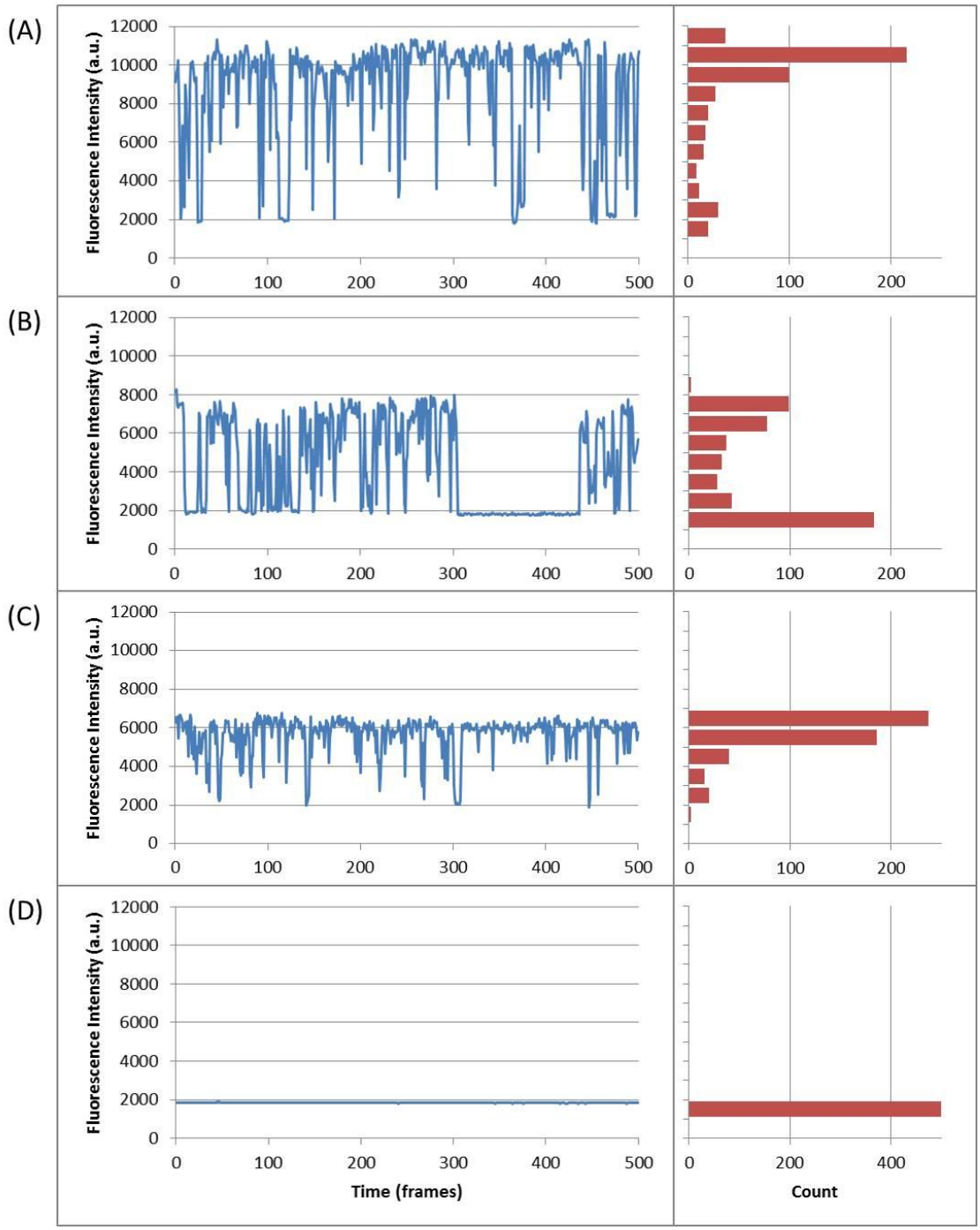


**Figure 3.1: Typical fluorescence time traces of single QDs.** (A – C): Each trace shows the average intensity of a 3x3 pixel area corresponding to one QD in an image, plotted over time. (D): Background. All samples are taken from the same image, displaying the varying behaviors of QD blinking and brightness. Image was recorded as 500 frames at 30.5 ms exposure, 32 frames/sec (total ~15 sec). Histograms at right are the distribution of intensities over time; bin size is 1000 fluorescence units, aligned with the y-axis for the time trace plots. Streptavidin-QDots 585, illuminated by 488nm laser at 50mW power.

The various behaviors illustrated in Figure 3.1 are typical of a sample of QDs, and several factors should be taken into account to explain this variety of signals. A set of QDs will be intrinsically poly-disperse, and the non-uniformities in particle size, shape and composition can contribute to the different observed signals. The examples here display differing maximum brightnesses, frequencies of blinking and extent of off-times. Blinking can result in off-times ranging from many seconds to times shorter than the camera frame rate – a range spanning four orders of magnitude. Not only do different QDs display different behaviors but also the same QD can have different behaviors over time. An additional source of variation in the intensity is the physical position of the QD in the sample during TIRF illumination. Due to the exponential decay of the evanescent wave, small differences in the distance from the glass surface can cause significant changes in illumination intensity. Inconsistencies in the sample surface, molecular motions, and different lengths of extension of the PEG surface molecules can all contribute to varying distances within the evanescent wave, resulting in different illumination and emission intensity.

A result of the inverse power-dependence is that the high probability of very short off-times can give rise to very fast blinking. When a QD is on for only a fraction of the 30.5 msec exposure time it will contribute a time-averaged intensity less than the maximum brightness. As seen in the histograms in Fig. 3.1, we observe two distributions of intensities around the means of the peak ‘on’-state and the background ‘off’-state instead of two fully distinct intensity levels.

As another source of intermediate fluorescence intensity states, it is possible that two QDs occupy the same diffraction-limited space. This coincidence would result in a different

characteristic behavior of three distinct states – two on, one on, or both off. This behavior is easily identifiable by a human observer examining the time trace, though the quantification of this type of signal is not trivial. However, this is a very rare occurrence and our analysis does not attempt to address it.

Several studies have attempted to reduce the blinking behavior by various means. Two general approaches are either engineering the QD core-shell structure and composition during the synthesis, or adding certain substances to the solution to suppress blinking during illumination. Blinking frequency has been shown to depend on the shell thickness, and blinking can be suppressed in QDs made with thicker or multi-layered shells (48, 50). Engineering the core-shell composition and creating a gradient shell instead of a distinct boundary can also lead to suppressed or non-blinking QDs (49, 51). Addition of certain compounds to the imaging buffer can help suppress blinking of ordinary QDs – especially thiol-containing compounds such as dithiothreitol or 2-mercaptoethanol, which are believed to alleviate the surface charge problem through their electron-donating nature (52, 53). But these methods are not without disadvantages. They can involve complex preparation and time-consuming syntheses or can cause other unusual fluorescence behaviors in the QDs – and most do not completely remove the blinking but just decrease it. Instead of considering these methods, we use commercially available QDs and focus on improving the detection and identification of the signal.

### 3.3 Detection of an Intermittent Signal

Considering these behaviors in QD intensity, the problem becomes how to detect such an unpredictable signal. The most obvious consideration is to expand the time of the

measurement. Under the inverse power-law behavior, as the observation time increases it becomes increasingly unlikely that a QD would have an off-time greater than the observation. Therefore, increasing the observation time increases the probability that fluorescence from any QD in the field of view will be captured. For most experiments using single QDs as reporters, researchers must collect fluorescence over more time than would be typically used in fluorescence imaging of organic dyes. Recording for a longer image sequence and using the average value over time has been a satisfactory method to collect signal from the QD reporters in the sample (28, 36).

Over longer time spans QD blinking can still be a problem. Bentolila (47) warns that due to the power-law behavior of on and off times, increasing the integration time will not increase the time-integrated brightness linearly, therefore it is difficult to use this practice as a means for reliable quantification. Crut (28) describes a method that takes a 60 sec measurement and then uses a combination of the average and maximum values over time, but still reports that QD blinking can cause difficulty for reliable detection.

For our QD detection image analysis, we expected to use a reasonably long observation time. Using the software ImageJ, a movie can be converted into a single image using various mathematical functions. This process, called Projecting, takes all the intensity values of a pixel through time and applies some mathematical operation to create a new image based on the result for each pixel over that time period. Several operations are available, such as the sum, average, maximum, or standard deviation. The result is then used as the value of this pixel in the new projection image, as illustrated in Figure 3.2. We can use this image for further processing and analysis to count individual particles. See Ch. 4 for a more detailed description

of QD detection in the projection images. For now, let 'detection' refer to the ability to distinguish a set of pixels corresponding to a QD as significantly higher than the image background.

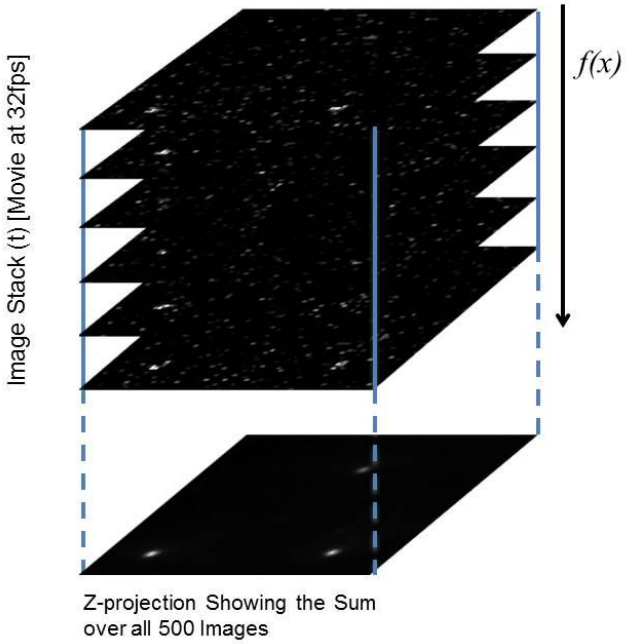


**Figure 3.2: Projection of an image stack.** The movie is a 4-dimensional object, with each x and y in the image plane having a pixel intensity changing over time. Each pixel is treated as a function of time and a mathematical operation is applied, such as the sum.

The method of stack integration is a useful solution to capture signal from QDs over time; however, the Sum Projection does not solve the issue of blinking. One could imagine that a QD that is in the 'off' state for most of the observation time will not be detected because its total signal might not be high enough to be easily separated from the total background. Returning to the statistics of the QD intensity over time, we consider other possible methods for stack projection. The Standard Deviation Projection would allow a means to detect QDs based on the distribution of intensity states instead of the overall signal. After comparing these different projection methods, the Standard Deviation Projection provides the best

signal/background ratio (SBR) and reveals the presence of QDs that would not be detected using simple integration. Figure 3.3 shows the two different projections taken from a small region of a sample data movie, with the time traces of the four QDs that are present in the region of view. As seen in the figure, there is a QD in the image that is not visible in the Sum projection because it is only on for a short time. The QD is visible in the Standard Deviation projection, highlighted in orange.

The SBR is greatly enhanced for QDs in the Standard Deviation projection compared with the Sum projection image. This result is shown in Figure 3.4, which shows the sum, maximum, and standard deviation values for each 3x3 pixel area corresponding to the QDs seen in the projections given in Fig. 3.3.

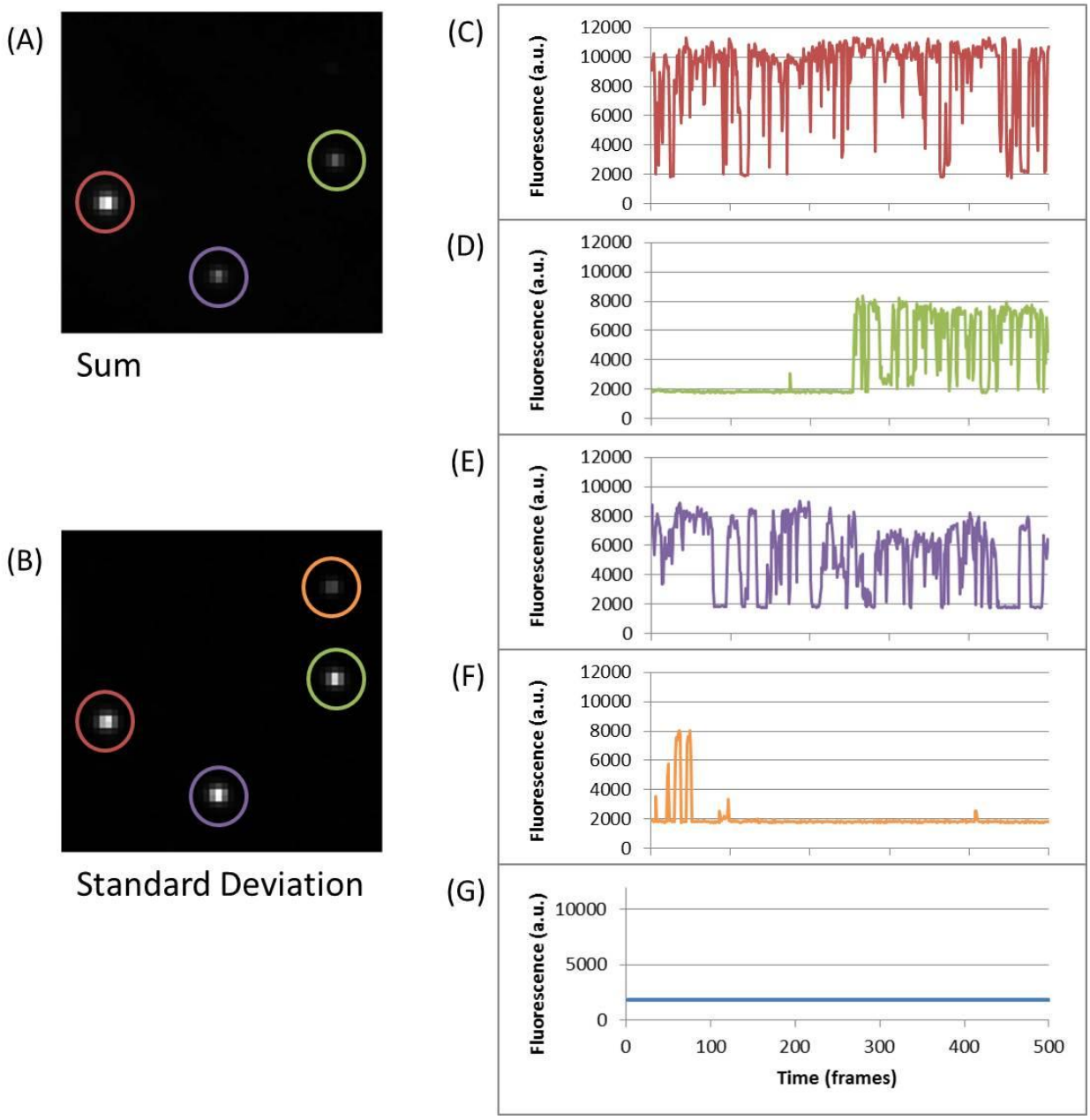


**Figure 3.3: Sum and Standard Deviation Projections for QD detection.** Sum projection (A) and Standard Deviation projection (B) of a region of interest, 13.8 um across, 1/100 of the field of view. A fourth QD is visible in the Standard Deviation projection that was not detectable in the Sum, highlighted in orange. (C-F): Fluorescence time traces for the QDs over the stack of 500 frames. Time traces were generated by the average value of a 3x3 pixel area corresponding to the QD position as identified by the Standard Deviation image. (G): Background time trace.

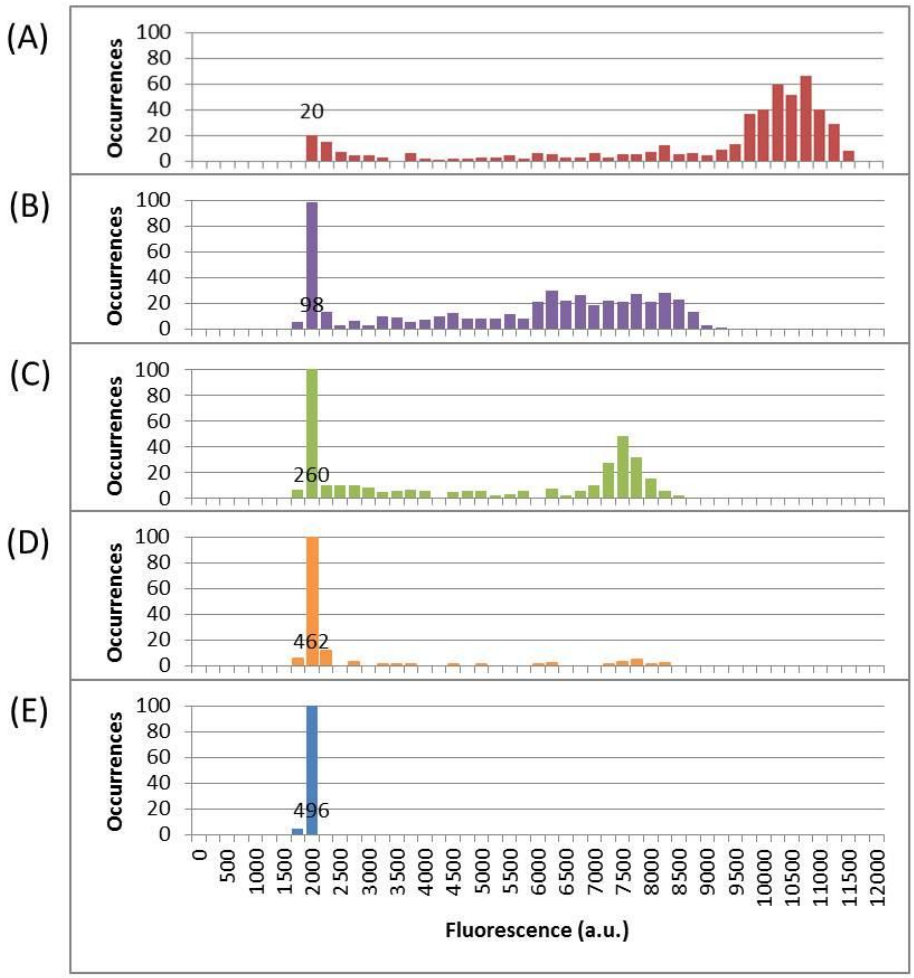


(F)

| | QD1 | QD2 | QD3 | QD4 | Background |
|---|---|---|---|---|---|
| Frames 'on' | 447 | 181 | 348 | 16 | 0 |
| Sum | 123.4 | 35.1 | 38.6 | 3.8 | 0.764 |
| /background | 161.5 | 45.9 | 50.5 | 4.9 | |
| Max | 136.4 | 81.4 | 106.9 | 74.2 | 2.320 |
| /background | 58.8 | 35.1 | 46.1 | 32.0 | |
| Standard Deviation | 90.3 | 74.9 | 101.7 | 26.4 | 0.771 |
| /background | 117.1 | 97.1 | 131.9 | 34.2 | |

**Figure 3.4: Histograms and statistics for blinking QDs with various z-projection methods.** (A-E): Histograms corresponding to the color-coded QDs highlighted in Fig. 3.3, binned by 250 fluorescence units. The y-axis is truncated, and the values for the counts at background level of 2000 are given in front of the bar for each histogram. (F): Statistics for the four QDs, giving the Sum, Maximum, and Standard Deviation of the 3x3 pixel area corresponding to the QD in each projection type. The number of frames 'on' was calculated as frames where the QD pixels were at least two times the background in intensity. Signal/background for each QD are given for the different projection types.

These figures demonstrate the ability of the Standard Deviation projection to greatly improve the SBR in images with QDs that are 'on' for even a very short time. While the Sum projection can give a high SBR for QDs with high overall 'on'-times, the SBR decreases significantly with increasing blinking. The broad distribution of the fluorescence intensity states creates a high standard deviation in the time-dependent signal. The Standard Deviation projection provides an image with better signal-background separation than the Max or Sum projections, as shown in Fig. 3.4(F) even for QDs with very short overall 'on'-times. In fact, increased blinking will actually enhance the signal in the Standard Deviation projection. It is important to note that although the Max projection can give high SBR as well, this method would be prone to inconsistent background levels, leading to widely varying SBR in different images as well as false positives if the background were high enough. Different images may have different background intensities, affecting the SBR for the Sum and Max projection methods. The Standard Deviation intensity for background levels will depend on the inherent noise in the sample measurement, which will be consistent between images.

The time traces and histograms given in the figures here show the variety of behaviors of QDs in a sample. Theoretically, the maximum SBR in a Sum projection would be obtained for a QD that is on for the entire observation time but will decrease for QDs that spend more time in the 'off' state. Conversely, the SBR in the Standard Deviation projection will increase with more blinking, as the pixels will display a wider distribution of intensities over time. We have seen that the Standard Deviation projection reveals QDs that were undetectable in the Sum projection, and this observation holds true when examining a large sample of QD populations.

Figure 3.5 compares the number of QDs counted in various projections, and illustrates the increase in QD detection when the Standard Deviation is used for stack projection.

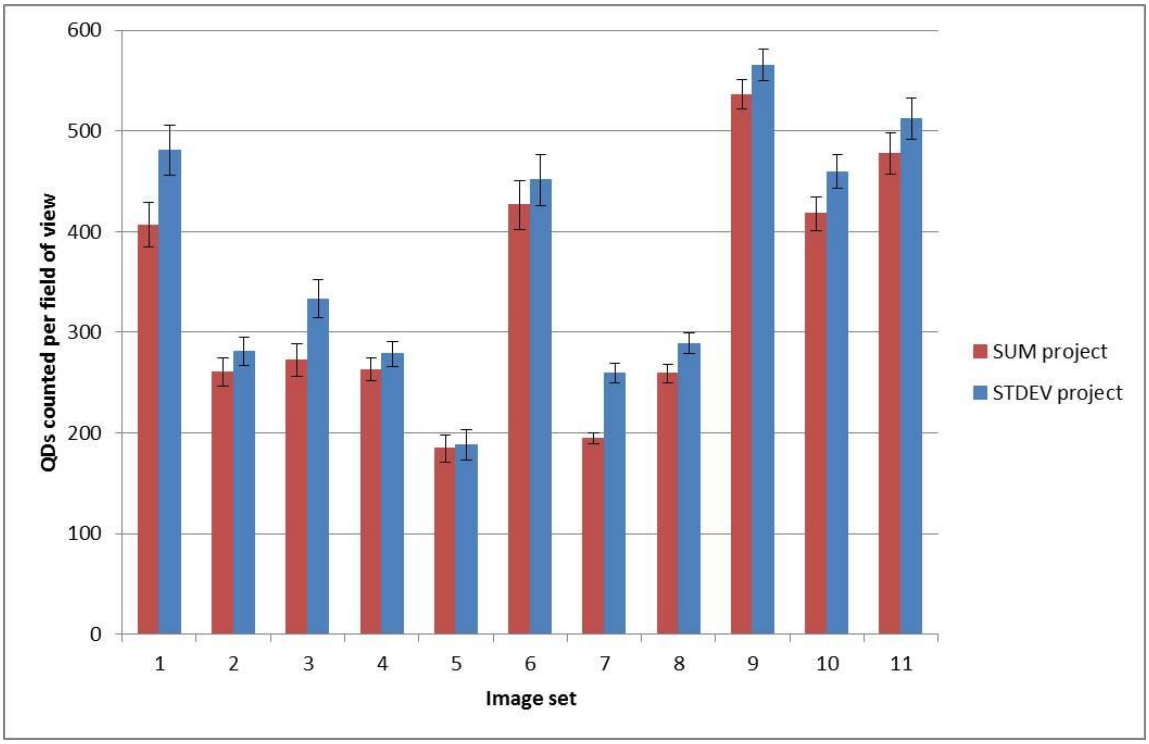


**Figure 3.5: Comparison of different projection methods for QD counting.** Red: QD counting for the Sum Projection, Blue: the same QD counting methods applied to Standard Deviation Projection. Each image set is seven images taken in the same SA-QD/biotin-PEG sample. Error bars show the standard deviation of the counts over the images in the set. The samples here are taken from various experiments at varying SA-QD concentrations to demonstrate the ability of the Standard Deviation projection over the Sum integration.

Incorporating the Standard Deviation into our image analysis improves QD detection by an average of 12% compared to simply using the Sum projection. The full image analysis and particle counting algorithm is described in Chapter 4. This method effectively addresses the varieties of QD blinking behavior and improves detection using a relatively simple tool for image analysis.

# 4. Image Processing and Analysis

## 4.1 Overview

All image processing and analysis were carried out using the open source Java-based software ImageJ (v. 1.44p, National Institutes of Health, http://imagej.nih.gov/ij). This section describes the steps in the image processing and analysis to determine the number of QDs in a sample field of view taken on the microscope. The image processing and analysis described here were automated in a self-written macro using ImageJ built-in functions. This automation provides a consistent analysis unbiased by a human counter while greatly reducing the time for analysis.

## 4.2 Image Processing

Image sequences were taken as described in Ch 2, 500 frames at 30.5 msec exposure time (~32 frames/sec) and converted into 16-bit depth multi-page TIFF movie files. To take advantage of the intermittent signal from QD reporters, we use the Standard Deviation projection instead of simply the Sum projection. This operation creates a projection image by calculating the standard deviation of each pixel's set of values through the stack (QD signaling and the advantages of Standard Deviation projection are discussed in Chapter 3). In order to improve detection of QDs with varying brightness and blinking behaviors, the Sum and Standard Deviation methods are both applied and the two resulting projections are normalized and merged into one composite image using the Merge Channels function. This process is illustrated in Figure 4.1 (the image used in the figures here is a subset of a data image, showing only a region 1/16 of the full field of view). Note that some particles are more prevalent in one

channel than the other. Combining the two projection methods was shown to increase QD detection by an additional 10 to 15% as compared to using a single projection. This composite image is then used for all following processing operations.

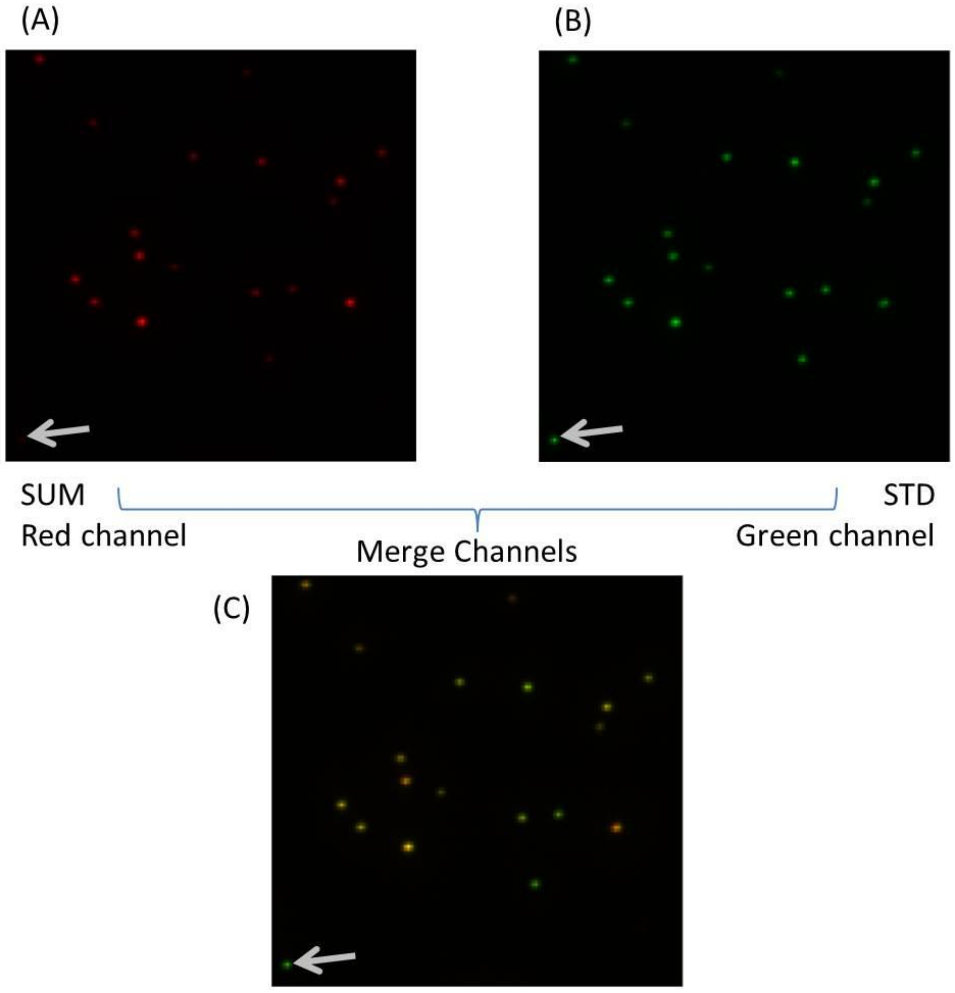


**Figure 4.1: Merging SUM and STD projections**. (A) and (B) are SUM and STD projections of the same sample image. (C) Merged image. Particles with a high Standard Deviation but low Sum appear more green in the merged image, while particles with a high Sum but low Standard Deviation appear more red. For example the particle at the bottom left (pointed by arrow), hardly visible in the SUM projection, is detected in the merged projection image due to its high signal in the STD projection.

The merged image is converted to an 8-bit grayscale image, preserving the overall intensity of each pixel but removing the color information. Next the Convolve tool is applied to enhance particle uniformity and further improve the signal/background in the image (see

Figure 4.2). This spatial convolution function works by multiplying a pixel and its neighbors by a kernel matrix [-1, -1, -1 | -1, 8, -1 | -1, -1, -1] and adding the results to calculate a new value for each pixel. The result is that pixels in and at the edges of bright particles are increased and pixels surrounded by low-level background are decreased. Figure 4.2 shows an image before and after applying the Convolve function, as well as a profile plot of a line traced across three QD particles. This convolution helps to separate signal from background and aids detection of particles in the image.

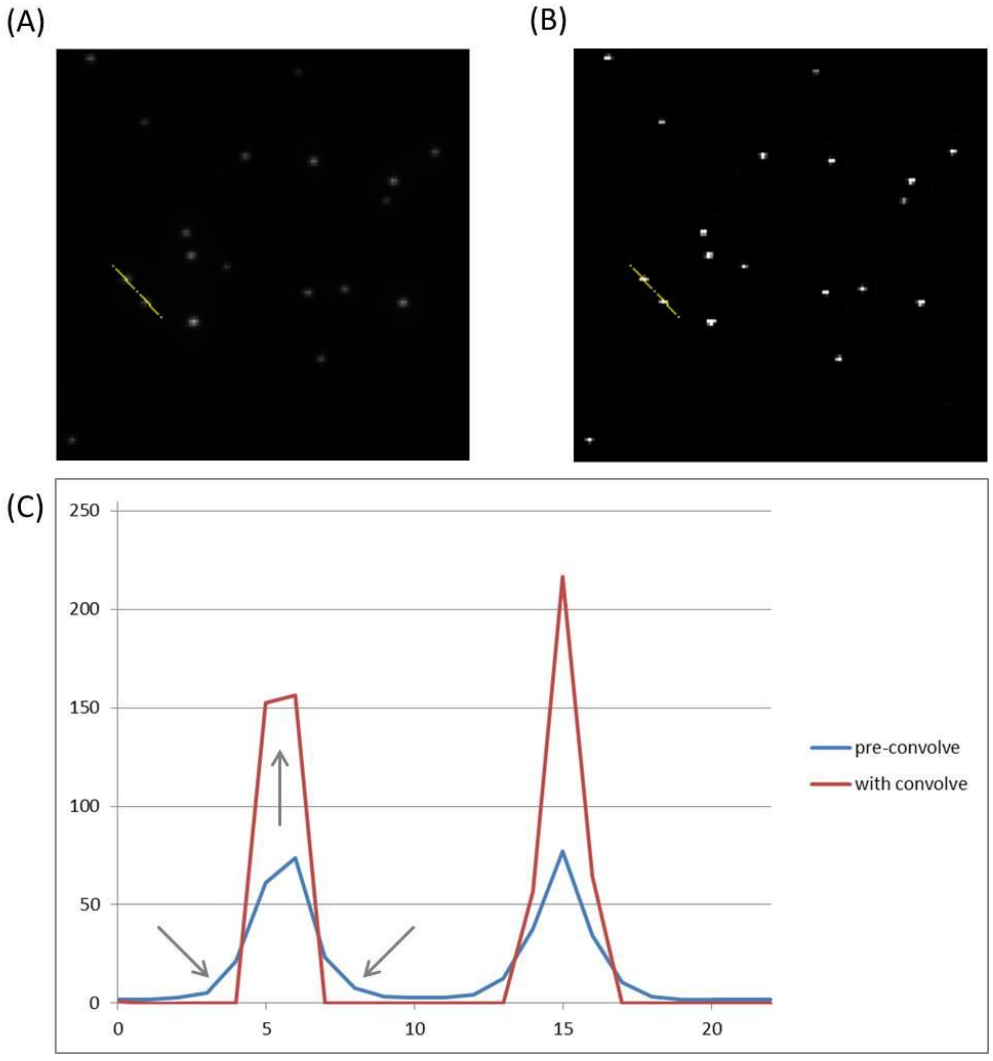

**Figure 4.2: Effect of Convolve function on an image of QDs.** The same image is shown before (A) and after (B) applying the Convolve tool. (C): The intensity profile along a line drawn through two QDs (yellow line in images A and B). Note the sharpening of the particle edges as well as the increase in maximum intensity.

The use of the combined Standard Deviation and Sum Projections as well as the Convolve tool gives higher QD detection than simply using a single processing tool. Ensuring a high SBR in the image enables more efficient counting and improved QD detection. As shown in Figure 4.3, the full processing yields 20 to 30% higher QD counts than using only the Sum or Standard Deviation Projections for particle counting analysis. The combination of the Sum and Standard Deviation projection methods ensures that QDs with different blinking behaviors are detected. The signal from QDs that spend most of their time in the on state will have a relatively lower standard deviation but still have a high sum, while QDs that blink frequently will have a low sum intensity but a high standard deviation.

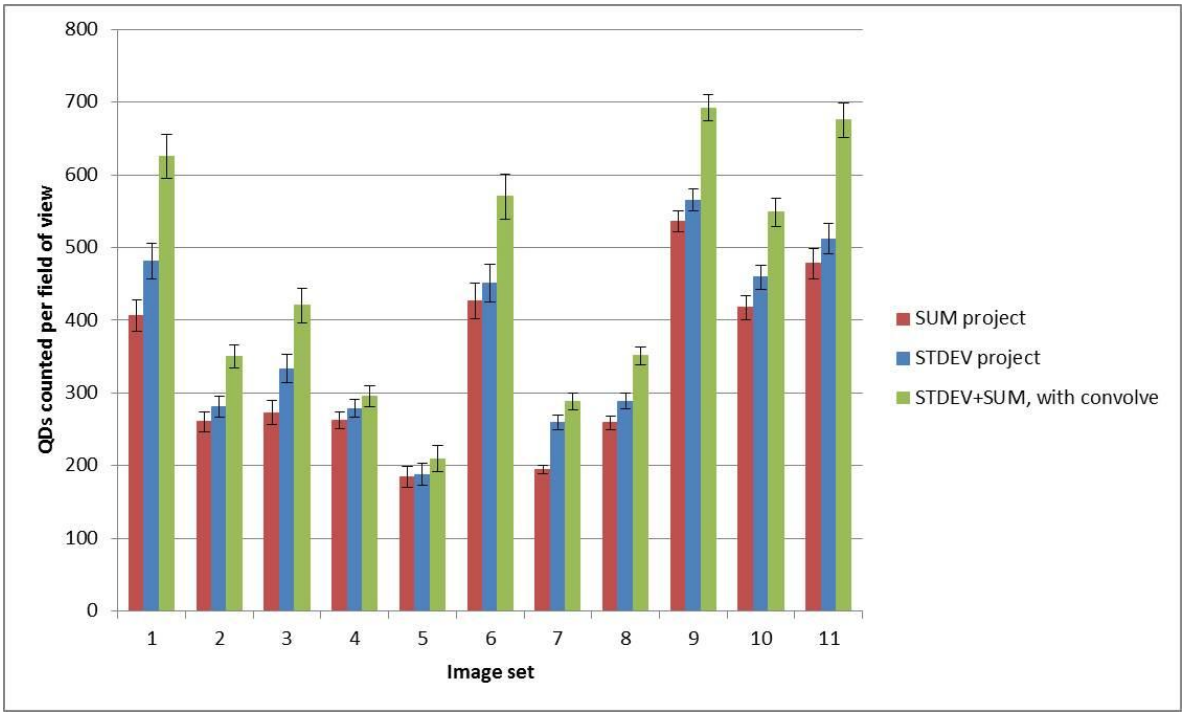


**Figure 4.3: Comparison of QD counting taking different image processing steps.** The same QD counting methods applied to (Red): Sum Projection; (Blue): Standard Deviation Projection; (Green): combined Sum+Standard Deviation projection with application of the Convolve function. Each set is seven images taken in the same SA-QD/biotin-PEG sample. Error bars are the standard deviation of the counts over the images in

the set. The samples here are taken from various experiments at varying SA-QD concentrations to demonstrate the ability of the image processing and analysis.

### 4.3 Threshold and Particle Counting

ImageJ has built-in functions Threshold and Analyze Particles to automatically determine the number of particles in the image. A particle is defined here as an object of a specified number of contiguous pixels above a certain intensity value. Because of the inherent variation in QD size, brightness and blinking behavior, the particles present in the images have varying sizes and brightnesses. To account for this variation and for variability between different images, I developed an algorithm for finding the optimal threshold level to maximize the amount of the image background excluded and the number of particles detected. In each image the particle size limit is set to count particles of size between 2 and 12 pixels. The expected size of a single QD was determined by the point-spread function to be 3x3 pixels, but this range allows for some variation in the QD population and defects in the images.

In a given image and for a certain particle size restriction, the number of particles counted depends on the threshold for several reasons. First, as the threshold is raised some particles will no longer contain enough pixels above the threshold to be counted as a particle (at least 3 pixels needed). At very low threshold, the image background can contribute significantly and cause an unrealistically high number of particles to be counted due to patches of background above the threshold. In the limit as the threshold approaches zero, the particle count decreases to zero as well, as very large patches or eventually the entire image would be counted as an object and will be above the size limit. As the threshold level is gradually increased we can see that fewer and fewer particles will be counted, as shown in Figure 4.4.

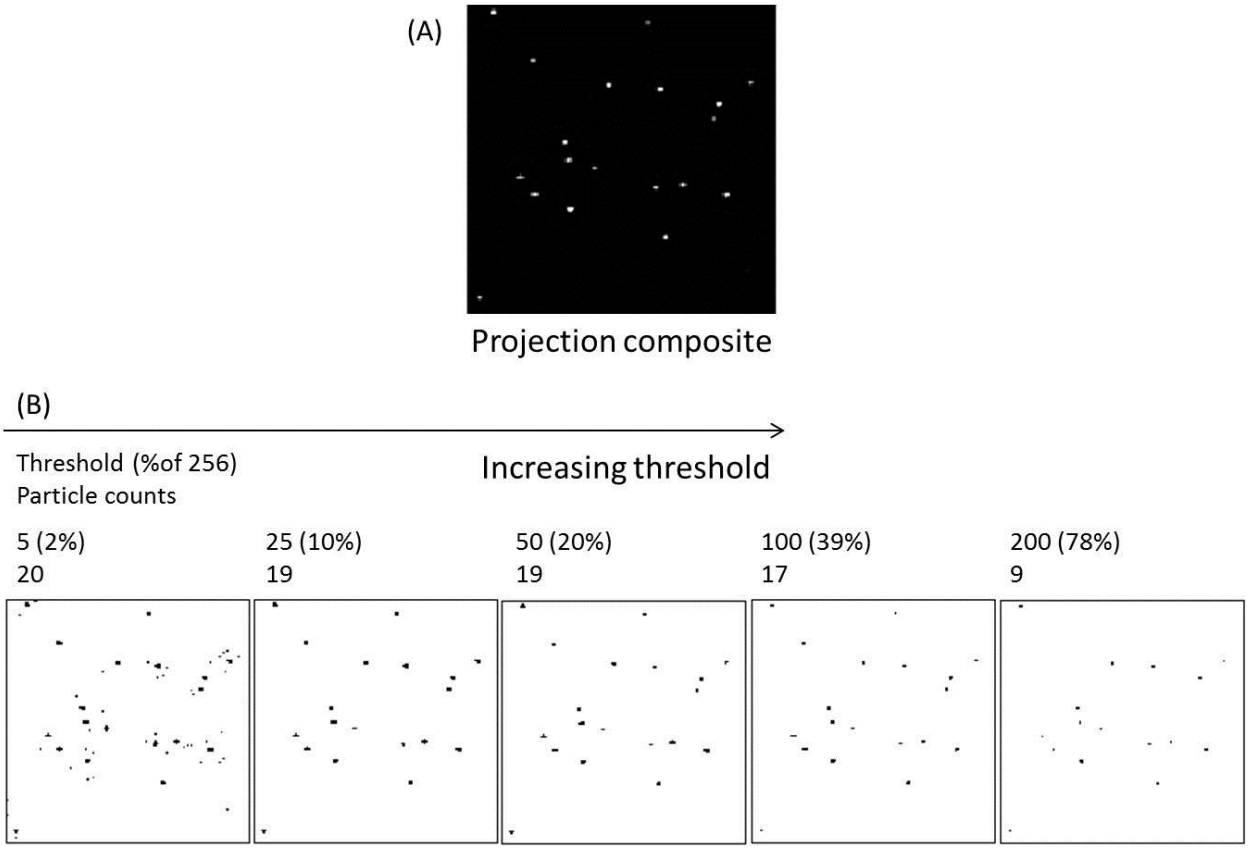


**Figure 4.4: Increasing threshold yields lower particle count.** (A): The same image sub-region used in Fig. 4.1 and 4.2, after the convolver has been applied. (B): As the applied threshold is increased, fewer particles are counted for the size range 2-12 pixels$^2$.

In each image there will be an optimal threshold level where most of the background pixels are eliminated while most of the QD particles are counted. This optimal threshold can vary depending on various characteristics of the image such as overall brightness, background level in the image and QD density and brightnesses.

### 4.4 Automation of Analysis in ImageJ Macro

The algorithm determines this optimal threshold for each image based on the set of particle counts across a range of threshold values. The program incrementally increases the threshold levels over the range from 2% up to 25% or 50% of the image brightness range stepping by 0.5% (the higher threshold values are included in images determined to have high

background levels). The Analyze Particle function is called at each threshold step, and the algorithm assesses the trend as particle count generally decreases with increasing threshold to select a window where the change in threshold gives the smallest change in particle count, usually a peak or a small plateau in the count as threshold is increasing. Figure 4.5 shows the variety of behaviors that can be seen in the dependence of particle count on threshold, and illustrates the binning and window selection used by the algorithm.

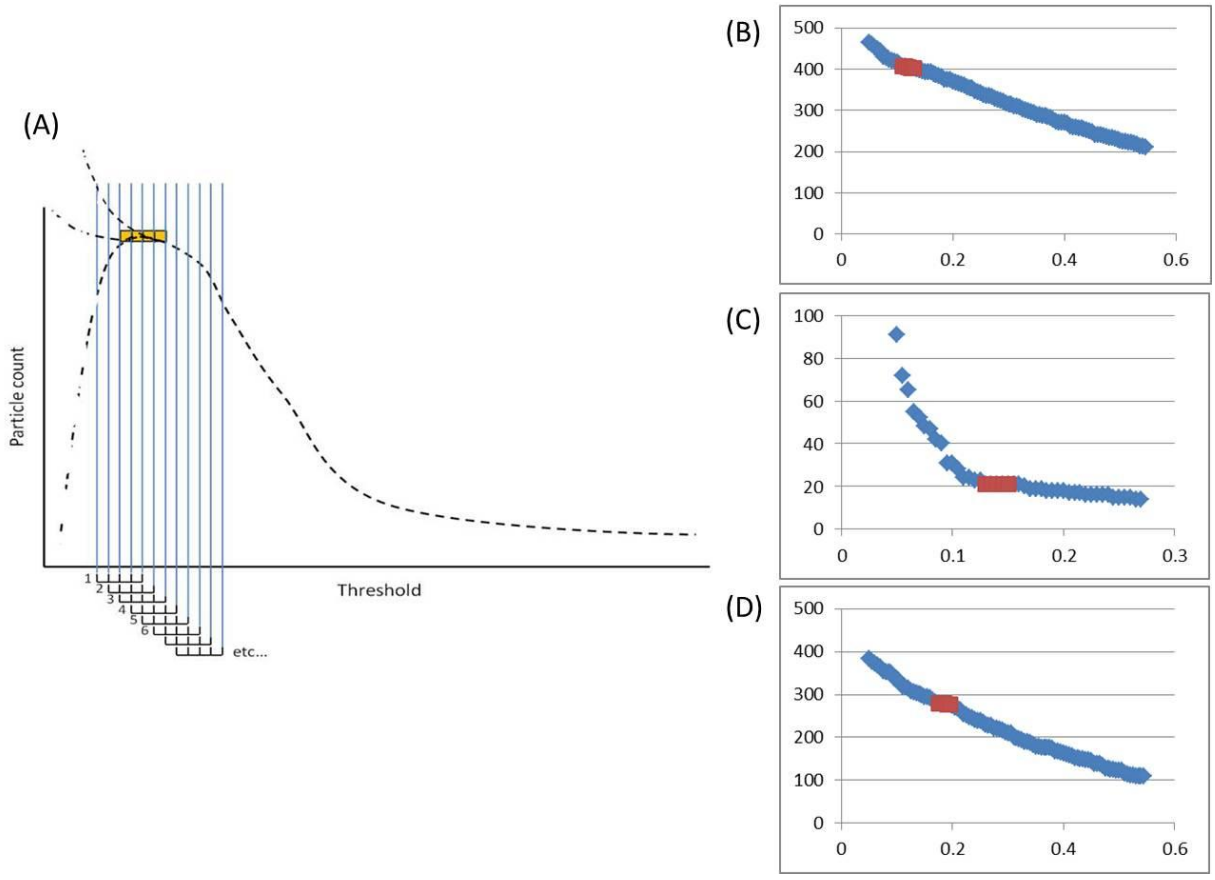


**Figure 4.5: Particle count vs. threshold behaviors.** (A): The algorithm selects the optimal threshold range based on the rate of change of particle count with threshold. The curve is exaggerated to illustrate the behavior as a peak or partial plateau. (B) – (D): A variety of behaviors of particle count vs. threshold, taken from data images. The 'optimal' threshold range as selected by the algorithm is highlighted in red for each.

Along this particle count vs. threshold curve, every point is addressed as the set of five consecutive steps. The difference between the counts at the first and fifth threshold values is

multiplied by the square of the threshold fraction corresponding to the center of the range. This result, termed the 'assessment value' is then compared for every five-step set of threshold intervals. The threshold set with the lowest assessment value is selected as the optimal range. This 'assessment value' is related to the rate of change on the particle count vs. threshold curve over a constant interval size. It is usually also observed that a subset of particles are of very high intensity and so the count vs. threshold curve flattens out in the upper limit (as in Fig 4.5), but this is not our desired count range. Multiplying by the square of the threshold fraction makes the algorithm more selective for count values in the lower threshold range. This extra preference is justified by comparison of automatic counts with manual counting of images, as this method gives results comparable to a human visual count for the images.

Regardless of the behavior of the count vs. threshold curve at low threshold, there is usually a range where the trend partially flattens or reaches a peak, and so the program assesses an incrementally moving range to find the window with the smallest change. When this optimum range is determined, the algorithm reports the average count value within this threshold range. The width of five steps makes the window a selection of 2.5% of the total range - more flexible than attempting to select a single value but still maintaining accuracy as compared to a human counter.

See Appendix 2 for the macro itself and a summary of the code.

## 5. Methods II: Development of a DNA Detection Assay

### 5.1 Overview

We would like to show that these improved QD detection methods can be applied in a biological detection scheme, such as an assay for nucleic acids. Taking advantage of the specific binding of complementary DNA strands, target molecules of a specific sequence can be captured on a surface and labeled with QD reporters and detected by TIRFM. Several experiments were performed to test various parameters and explore different chemistry and labeling strategies. Attaching a chemically modified DNA capture probe to the surface and adding a complementary modified signal probe, we can test various experimental conditions with a direct hybridization. Although this type of scheme is not ideal for a detection assay, it is useful to understand the experimental considerations required for experiments. The assay would more realistically use a non-modified DNA strand as a target, as in the sandwich scheme described in Figure 5.1. While the direct-hybridization experiments were not used to create a full calibration curve, various procedures for surface functionalization, hybridization, washing, blocking, and QD labeling were investigated. Recent experiments have been carried out to assess the parameters for a successful DNA sandwich assay.

### 5.2 Design of the DNA Assay

Two surface chemistries were proposed for covalently linking the capture DNA probe to the surface: a poly-glutamic acid monolayer and EDC/Sulfo-NHS coupling with amine-modified DNA capture probe (54), or a maleimide-PEG surface with thiol-modified DNA capture probe. Samples using the maleimide-PEG surface were compared with samples using the poly-glutamic acid chemistry prepared by lab member Stephanie Schubert. The thiol-DNA/maleimide-PEG

scheme was chosen because it was an easier preparation, similar to the earlier biotin-PEG experiments, and gave slightly better binding efficiency. It also allows control of the density of surface binding sites, by the ratio of maleimide-PEG to methoxy-PEG. This scheme was used for subsequent experiments and methods for preparation are given below in section 5.3.

For hybridization conditions, two alternatives were considered. Based on previous work by lab members, two hybridization buffers were proposed: 4x PBS buffer or 4x SSC buffer. Results comparing these two buffers indicated the 4x PBS provided modest improvement in binding efficiency and sample consistency.

Another important consideration for the experimental design is the linkage of the signal probe and QD reporters. Two often-used schemes are to covalently link the DNA probe to the QDot surface (30, 55), or to use biotin-modified DNA probe and streptavidin-conjugated QDs (28, 29, 47). These two methods have significantly different behaviors to consider and each has advantages and disadvantages. First, QDs covalently linked to DNA (DNA-QDs) could allow for easy multiplexing as different sequence signal probes could be conjugated to different color QDs for labeling and detection of multiple targets in the same sample. The increased stability of the covalently linkage gives the possibility that DNA-QDs could be prepared in batches and stored for later use, and would also be more stable in experiments, whereas the non-covalent biotin-streptavidin method will have some unbinding after a certain time (2). Additionally, the preparation of DNA-QDs will result in QDs with many DNA strands attached to the surface. This will create a high local concentration around a QD as it diffuses to the sample surface and could enhance the likelihood of hybridization. Because the DNA probes are attached to the relatively larger QD, the rate of diffusion will be significantly slower than for free DNA probes in solution.

Because the DNA hybridization has a binding constant ($K_h$ ~$10^9$ $M^{-1}$ for short oligonucleotides) (56) than the biotin-streptavidin interaction ($K_a$ ~$10^{11}$ to $10^{15}$ $M^{-1}$) (2), we would like to place the kinetic barrier of QD diffusion on the more thermodynamically favored step. Using the biotin-DNA/SA-QD scheme will also be analogous to previous experiments using SA-QDs binding to biotin immobilized on the surface: here, the biotin has been immobilized via a hybridization event.

Additionally, the DNA-QD functionalization reaction will yield a distribution of DNA-QD products with varying numbers of DNA probes per QD and this distribution will be difficult to control. In contrast, using separate biotinylated DNA signal probe and streptavidin-QDs will allow better control of the ratio of DNA to QDs in the sample. This scheme would separate these variables and allow more careful control of parameters for DNA hybridization and QD labeling in terms of time, concentration and other conditions.

DNA-QDs prepared by lab member Stephanie Schubert were used in comparison with the biotin-DNA/SA-QD scheme. The DNA-QDs were prepared by EDC/Sulfo-NHS coupling of amine-modified DNA probe and carboxylated QDs. Several brief experiments were performed to compare binding efficiency and non-specific binding of each method and to assess the stability of stored DNA-QDs. As expected, the DNA-QDs required a longer hybridization time than biotin-DNA probes to achieve comparable binding signal, but also had higher non-specific binding. Additionally, using the DNA-QDs a week or more after preparation resulted in poorer performance (lower binding efficiency and higher non-specific binding), likely due to degradation during storage. The DNA-QD conjugation reaction is time-consuming and because these results did not indicate significantly better performance, the DNA-biotin/SA-QD scheme

was chosen for subsequent experiments and is further described here. This separation of steps will also allow further control of individual components in later work for optimizing the assay's labeling efficiency and minimizing background. The overall scheme proposed for the DNA sandwich assay is given below in Figure 5.1.

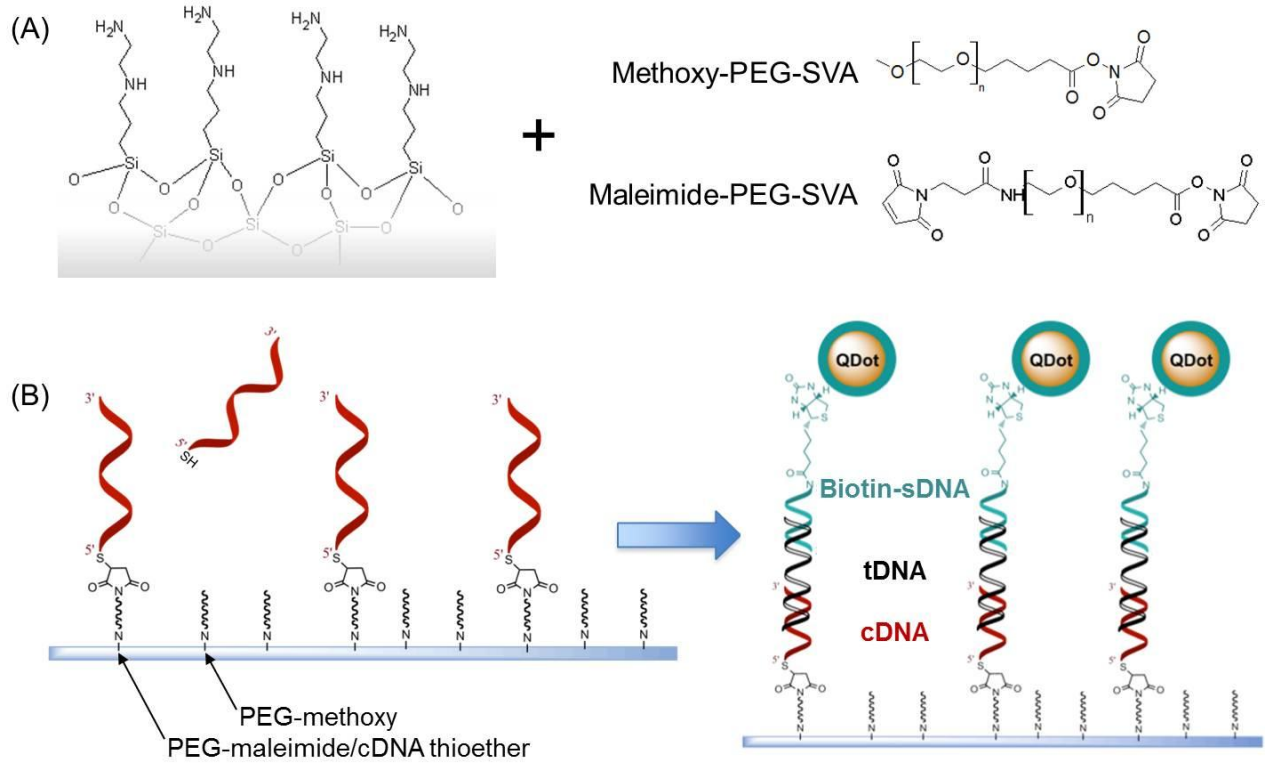


**Figure 5.1: Surface chemistry and DNA sandwich assay scheme.** (A): Amine-modified glass reacts with a combination of methoxy- and maleimide-PEG-SVA reagents. (B) Thiol-modified DNA (red) reacts with maleimide groups on surface and is used as a capture probe for target DNA (black). Biotinylated signal probe DNA (green) binds to captured target, and then SA-QD reporters are used to signal capture events.

## 5.3 Immobilization and Detection of DNA Oligonucleotides Using SA-QDs

### *5.3.1 Materials and Methods: Thiolated DNA on Maleimide-PEG Surfaces*

Sequences for the DNA probes used, taken from the *E. coli* GAPDH gene, are given below in Table 5.1. Probes were purchased from IDT Corp. The biotinylated signal probe (biotin-sDNA) contains a dual-biotin modification. Two biotin molecules are attached together at the 5' end of the probe; the distance between the biotin molecules is close to the distance

between the multiple binding sites of the streptavidin protein, resulting in a stronger binding interaction. Both the signal probe and capture probe are 23 nucleotides long. They have fully complementary regions on the target probe, separated by 15 nucleotides.

Table 5.1: Oligonucleotide probe sequences.

| | |
|---|---|
| Target DNA (tDNA) | 5'-GGA AGG TGA AGG TCG GAG TCA ACG GAT TTG GTC GTC ATG GCC CAC ATG GCC TCC AAG GAG TAA GA-3' |
| Capture probe (cDNA-S) | 5'-/5ThioMC6-D/ TTA CTC CTT GGA GGC CAT GTG GG |
| Signal probe (biotin-sDNA) | 5'-/52-Bio/CCG TTG ACT CCG ACC TTC ACC TT |

Samples were prepared on 384-well plates, using procedures similar to those described in Chapter 2. Wells were cleaned by filling, mixing and removing solutions via pipette: ultrapure water (Sigma), 5% Alconox solution (washed three times with water after), isopropanol, 1M KOH for 10 minutes, and ultrapure water. Silanization was carried out with N-(2-aminoethyl)-3-aminopropyl trimethoxysilane (AE-APTMS), with a mixture of 25 mL methanol, 1.25 mL acetic acid, and 0.25 mL AE-APTMS. 50 µL of this solution was added to each well and allowed to react for 20 minutes. The PEG solution was prepared using 5 mg methoxy-PEG-SVA (MW 2000) and 0.42 mg maleimide-PEG-SVA (MW 3400) per 100 µL of 0.1 M $NaHCO_3$ solution, mixed thoroughly and centrifuged at 7200*g* for 1 minute to remove bubbles. 40 µL of this solution was added to each well and allowed to react for one hour and then this reaction mixture was replaced with freshly prepared reaction mixture for one more hour. After the reaction, wells were washed with ultrapure water (Sigma).

Thiolated DNA capture probes (cDNA-S) were prepared by cleaving the disulfide-linked $C_6$ protecting group by reduction with Tris(2-carboxyethyl)phosphine hydrochloride (TCEP·HCl).

50 µL of 50 mM TCEP·HCl (dissolved in 1x PBS) and 50 µL of 100 µM cDNA-S-S-C6 were mixed and allowed to react for 30 minutes. The reaction product was separated from the mixture using a Centri-Spin-10 column (Princeton Separations), centrifuging at 750*g* for 2 minutes. The concentration of purified cDNA-S was determined using Nanodrop UV-Vis at 260 nm. cDNA-S was then diluted to 3 µM in 1x PBS, and 50 µL of 3 µM thiol-DNA solution were added to each well and allowed to react for 2 hours. After this time the wells were rinsed and re-filled with 1x PBS and stored overnight in the dark at $4^{o}$ C.

The following steps are still being tested to find optimal conditions for the sensitivity response and limit of detection for the assay. Target DNA (tDNA) is prepared in various concentrations in hybridization buffer (4x PBS) and 100 µL is added to each well and allowed to hybridize for some time. The tDNA solution is removed and the sample is washed by pipette three times with a low stringency wash, 2x SSC (contains 0.3 M NaCl and 0.03 M sodium citrate) and 0.2% sodium dodecyl sulfate (SDS), followed by a high stringency wash, 0.05x SSC (contains 0.075 M NaCl, 0.0075 M sodium citrate). Then wells are rinsed once with 1x PBS before adding the signal probe DNA. Biotinylated DNA signal probe (biotin-sDNA) is prepared at a certain concentration in hybridization buffer (4x PBS) and 100 µL is added to each well and allowed to hybridize for 4 hours. The same washes are used, three times with 2x SSC/0.2% SDS followed by three times with 0.05x SSC. Wells are rinsed once with 1x PBS and then surfaces are blocked by adding 100 µL of 1% BSA (in 1x PBS) for one hour. The SA-QDs are prepared at 0.5 pM concentration in 1% BSA blocking buffer. Blocking solution is removed from the wells and 50 µL of the SA-QD solution is added to each well and allowed to bind for 30 minutes. After this time

the wells are washed three times with 1x PBS and refilled with 1x PBS for imaging. Imaging, analysis and QD counting are carried out as described previously.

*5.3.2: Results and Discussion*

Preliminary experiments to collect data for calibration across a range of target DNA concentrations have been unsuccessful, with initial experiments showing weak correlation of QD count with tDNA concentration as well as high nonspecific binding. Other experiments have been performed to assess the contributions of the various factors to the performance of the assay. First, experiments with no target DNA were prepared to assess the dependence of non-specific binding on the signal probe concentration and SA-QD concentration. We expected that the nonspecific binding of SA-QDs would be an important factor to the background signal of the overall detection scheme. Samples were prepared with three different concentrations of biotin-sDNA (1, 5, and 10 pM) and three concentrations of SA-QDs (1, 0.7, and 0.4 pM). Two experiments were performed, one with a 4 hour biotin-sDNA incubation time simulating the hybridization time and one with 7.5 hour incubation time. The two experiments gave very similar results and the results from the 4 hour set are shown in Figure 5.2, showing the number of QDs counted as a function of both SA-QD concentration and biotin-sDNA concentration.

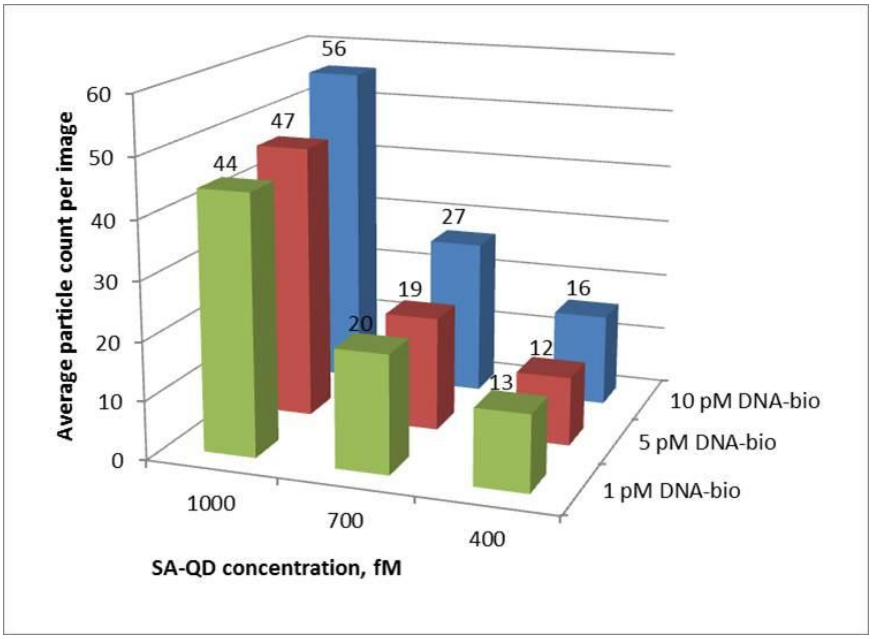


**Figure 5.2: Nonspecific binding as a function of SA-QD concentration and biotin-sDNA concentration.** Samples contained no target DNA, but only biotin-sDNA and SA-QDs at the indicated concentrations.

The observed number of QDs has a much stronger dependence on the SA-QD concentration than on the biotin-sDNA concentration, suggesting that the overall nonspecific binding is mainly affected by the SA-QD concentration. For future experiments we decided to use a low concentration of SA-QDs such as 500 fM with a higher biotin-sDNA concentration, such as 5 or 10 pM. Knowing that the nonspecific binding depends mainly on SA-QD concentration and is only weakly dependent on the biotin-sDNA concentration and hybridization time, we designed another experiment to test the response with target DNA to find the range of concentrations that will ensure efficient capture and labeling.

For this screening experiment the key variables were hybridization temperature (room temperature or 36$^{o}$C), target DNA incubation time (4 or 12 hours), and biotin-sDNA concentration (5pM or 50pM). Samples were prepared as described above, with all possible combinations of these factors. Target DNA concentration was 250 fM and SA-QD concentration

was 500 fM for all samples. The results are given in Table 5.2 below. All samples were prepared in duplicate and the average count per field of view across 8 images in each of both samples is reported.

| Hybridization Temp, $^{o}$C | Target incubation, hr | Biotin-sDNA concentration | Average counts |
|---|---|---|---|
| 24 | 4 | 5 pM | 302.4 |
| 24 | 4 | 50 pM | 353.0 |
| 24 | 12 | 5 pM | 187.7 |
| 24 | 12 | 50 pM | 182.6 |
| | | | |
| 36 | 4 | 5 pM | 148.0 |
| 36 | 4 | 50 pM | 158.5 |
| 36 | 12 | 5 pM | 78.7 |
| 36 | 12 | 50 pM | 85.9 |

**Table 5.2: DNA assay parameter screening experiment.** The average count given is number of particles per field of view for two samples at each set of conditions. Target DNA concentration was 250fM and SA-QD concentration was 500fM for all of these samples.

These results indicate the overall signal has a strong dependence on hybridization temperature and target incubation time, with little dependence on the signal probe concentration at the conditions tested. Further experiments are in progress to re-assess the nonspecific binding at these conditions, and to ensure these conditions have a sensitive response over a wide range of target DNA concentrations.

# 6. Extensions, Future Work and Conclusions

## 6.1 Incorporation of QD-based Detection into a Microfluidic Device

We hope to apply the single molecule detection methods developed here as a readout scheme in a microfluidic device for more complex analysis of biological samples. Microfluidic platforms provide several advantages, allowing a high level of control of very small sample volumes. In this project, several experiments have been attempted to demonstrate the possibility of using similar capture and detection schemes in a microfluidic device. Illustrated in Figures 6.1 and 6.2, we designed a set of PDMS devices to enable spatially separated detection zones by successively overlaying different sets of channels on the glass surface.

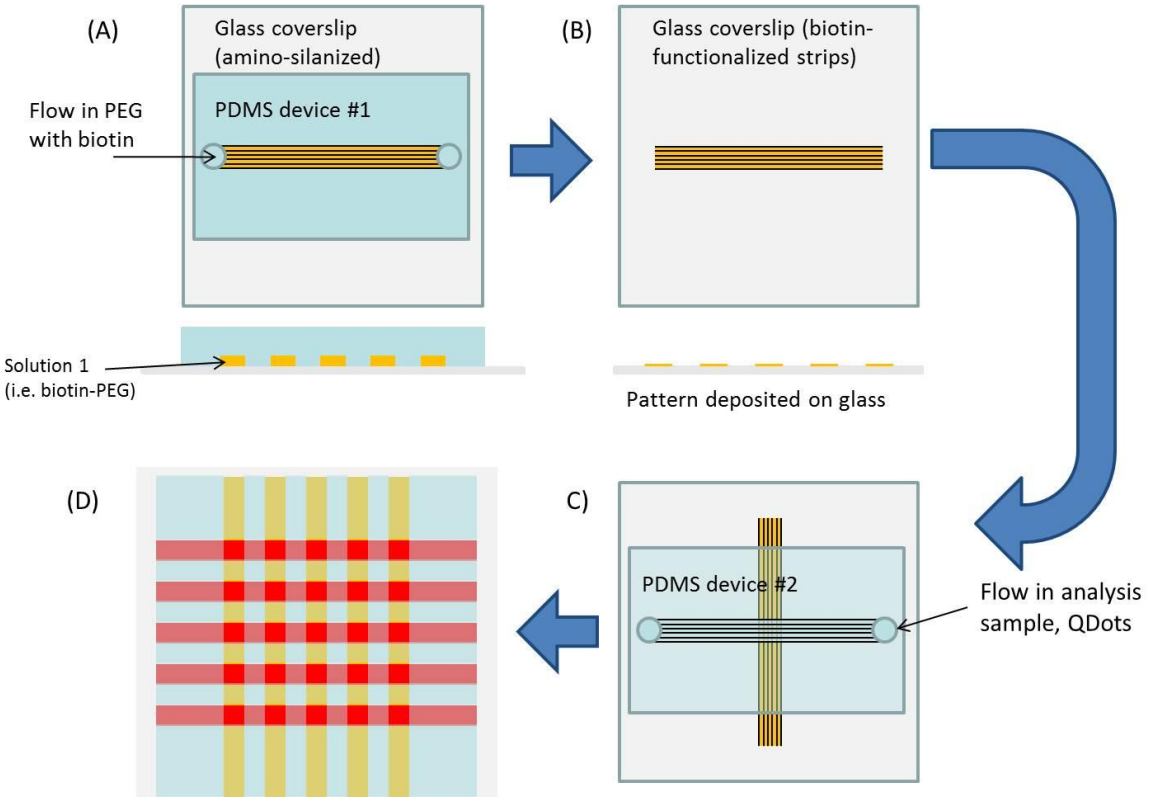


**Figure 6.1: PDMS Channels for creating spatially separated sensing patches in a microfluidic device.** The first set of channels carries the surface functionalization reagents (A), only modifying strips on the glass surface (B). Then a new set of channels are laid across the surface pattern (C) and the sample is flowed through these channels, passing over discrete patches of capture sites (D). The resulting patches are 100 um x 100 um, but can be modified to be other sizes by using different sized channels.

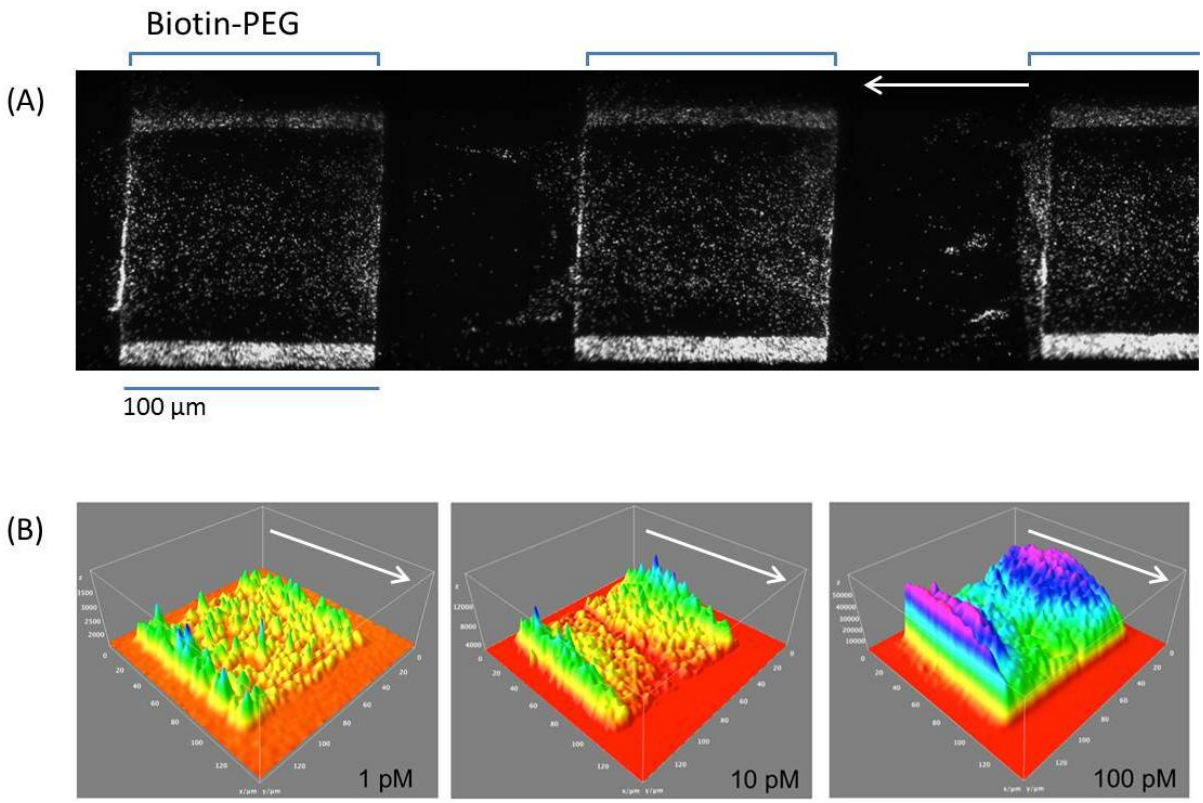


**6.2: Detection patches created in microfluidic device.** Patches of biotin-PEG were deposited using the microfluidic channels as described in Fig 6.1. (A): Three detection patches are shown in this stitched image, specifically functionalized with biotin-PEG. SA-QDs were flowed at concentration of 1 pM for 30 minutes. Arrow indicates direction of flow. (B): False-color 3D projections of fluorescence intensity corresponding to patches in different channels with SA-QD concentration 1, 10 and 100 pM. Arrow indicates direction of flow.

These results indicate that with some improvements, this method could be used to create distinct zones of specific surface functionalities. This method could potentially be expanded for spatial multiplexing with the sample being exposed to different surface modifications at each patch. Although the results here look promising, the method can be difficult and time-consuming. Sealing the functionalization device onto the glass often fails and this should be an area to improve if the method is to be developed into a consistent and reliable device. It was also difficult to control the rate of flow, although this control could be improved by using a pump instead of adjusting the flow by hand. As seen in Fig. 6.2, there may be some inconsistencies in the surface functionalization and binding density due to the flow

dynamics. This problem might be alleviated by better controlling the flow at a constant rate or by stopping the flow and allowing the reaction and binding to occur under the stationary fluid.

### 6.2 Single Enzyme Kinetics Studies

A very interesting possibility is using the TIRFM platform to study enzyme kinetics at the single molecule level. If single β-Galactosidase enzymes (β-Gal) were captured on the glass surface, we could observe individual catalysis events as the fluorogenic substrate resorufin-β-galactopyranoside is cleaved, as in Figure 6.3. TIRFM should have sufficient resolution and sensitivity to observe fluorescence from single resorufin molecules, collecting kinetic data for individual enzyme molecules.

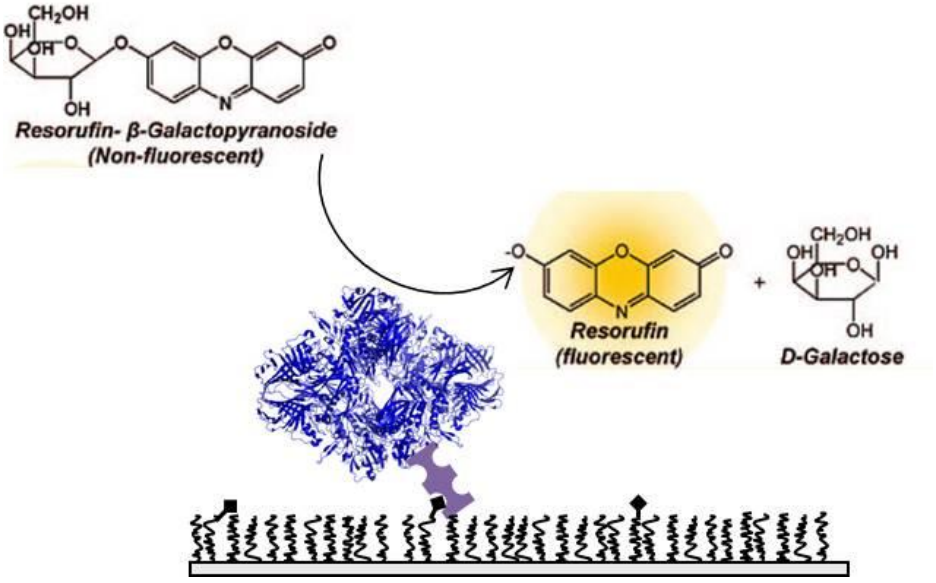


**Figure 6.3: Possible scheme for monitoring single β-galactosidase enzyme activity on TIRFM platform.** Streptavidin-β-Gal can be captured at the surface via biotin. As the non-fluorescent substrate is cleaved to form resorufin by individual enzyme catalysis events, fluorescence can be observed by TIRFM.

This approach could be used for basic kinetics studies of β-Gal enzyme or could possibly be developed to use the enzyme as another stochastic reporter instead of QDs. Preliminary

experiments appeared successful in detecting fluorescence from individual catalysis events. Sample data are shown below in Figure 6.4. Streptavidin-conjugated β-Gal enzymes were immobilized in wells treated with biotin-BSA, along with a very low number of SA-QDs added to visualize the surface with TIRFM. Then resorufin-β-galactopyranoside solution was added to the solution in the well while recording a TIRFM movie of the surface. The stack projections can be used to select regions of interest as a 3x3 pixel area corresponding to a repeatedly active enzyme and then the intensity time trace of that selection is analyzed through the stack. Many β-Gal enzymes can be monitored in parallel in the field of view.

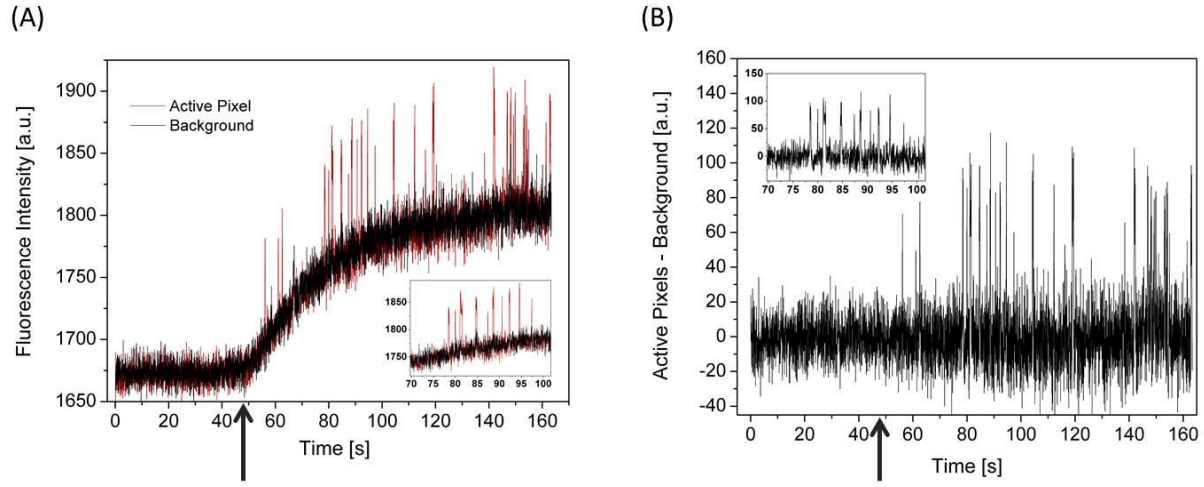


**Figure 6.4: Time trace of fluorescence intensity for single β-Gal enzyme.** (A): Raw fluorescence for 3x3 pixel selections of background (black) and pixels corresponding to an active enzyme (red). (B): Active pixel intensity minus background (for the same data as in A). Arrow indicates the time of substrate addition.

Although these results appear successful, it became clear that the time-resolution of the camera and also the background fluorescence of resorufin throughout the sample solution were significant issues. The β-Gal kinetics are faster than the timescale of the camera exposure (up to several hundred molecules/sec turnover rates have been reported (1), compared to the 32 frames/sec of our recording), possibly resulting in multiple catalysis events being indistinguishable. Due to the excess of substrate needed to achieve steady-state conditions at

the surface, a large amount of resorufin is produced in the well and contributes to a background level of fluorescent molecules diffusing into the TIRF excitation volume. It becomes difficult to distinguish between pixels with fluorescent burst events due to enzyme activity and pixels with fluorescence due to diffusion of already-produced resorufin back into the excitation volume.

Several possible solutions could be explored to alleviate these problems. A faster camera could be used to gain higher time resolution, or the current camera's settings can be changed to allow faster frame-rates at the expense of sacrificing the image size. To help eliminate background fluorescent molecules, the assay could be performed in a microfluidic channel with a constant flow. This flow would serve both purposes of removing reaction product and keeping a fresh supply of constant-concentration substrate solution. Also we could try to slow down the enzyme rate by using modified substrates or additives in the reaction solution, or by choosing a different enzyme to study that does not have as high an activity as β-Gal.

### 6.3 Conclusions

The procedures developed in this thesis demonstrate the capability of a TIRFM platform for digital quantification of single molecules. Preliminary experiments have shown limits of detection around 1 fM for measuring streptavidin-conjugated Quantum dots on a biotin-functionalized surface, although the assay could be modified to allow detection at even lower concentrations. Importantly, our method takes advantage of the intermittent fluorescence that has proved to be a problem for most single molecule detection applications of QDs. Instead of

simply measuring the total signal over time, the standard deviation of the time-dependent signal is used to generate image data for QD counting, improving detection of QDs by up to 20%. The particle counting algorithm accounts for the inherent variability of QD blinking behaviors and variations between images, and greatly reduces the time for analysis and provides an effective and consistent counting method. The QD detection methods have been applied in developing an assay for DNA detection. Although the full assay has not been successful, current and future experiments are focused on selecting the optimal conditions for DNA capture, signal probe hybridization, and QD labeling.

## Appendix 1: Protocols for sample preparation

1: Biotin-PEG-SVA surface prep for Streptavidin-conjugated Quantum Dots in PDMS well mounted on glass coverslips.

Coverslips: Use 1.0 weight. If using microfluidics clamp will need to use 25x25mm or smaller coverslip size. If using PDMS wells can use larger size coverslips if it's easier.

Cleaning: In *glass* staining dish, sonicate with the following wash solutions, be sure to rinse well enough in between and use enough reagent to completely cover the glass slides:

1. 10% Alconox suspension – 20 min
2. Water (MilliQ) – 5 min (rinse well to remove Alconox soap bubbles)
3. Acetone – 10 min
4. 1M KOH – 15 min
5. Water (MilliQ) – 10 min

Can store cleaned coverslips individually in MilliQ water in 50 mL Falcon tubes, for a week or so.

Silanization: APTES or similar silane (e.g. N-(2-aminoethyl)-3-aminopropyltrimethoxysilane).

1. Remove slides from water, dry under $N_2$.
2. Clean glassware and rinse with methanol. Be sure to remove all water from glassware and slides.
3. Prepare a 1% silane mixture with: (or scale up volumes if more is needed to cover all slides. 50mL is plenty for one staining dish)
    a. 50 mL methanol
    b. 2.5 mL acetic acid
    c. 0.5 mL APTES (or other silane)
4. Mix silane solution well in a beaker and immediately add to slides in a *plastic* staining dish.
5. Allow to react for 20 minutes. After the first 10 minutes sonicate for 1 min (and continue reaction for last 9 minutes).
6. Remove reaction solution and replace with methanol.

Assembly of PDMS wells onto glass:

1. Cut piece out of PDMS, big enough to fit two wells side-by-side but not larger than the glass coverslips. Punch well holes with hole-puncher (7mm diameter)
2. Clean PDMS pieces briefly swabbing with ethanol and then plasma treat.
3. Remove PDMS from plasma and immediately place cleaned, silanized, and *thoroughly dried* (in $N_2$) glass coverslip on the plasma-treated face of the PDMS. Press and allow PDMS piece to adhere.

PEGylation: (SVA has a short half-life in aqueous solution (~30 min) so prepare the solution and use immediately)

1. 40:1 ratio of mPEG-SVA:Biotin-PEG-SVA. Concentration used is

a. 12.5 mg mPEG-SVA
b. 0.31 mg biotinPEG-SVA
c. Per 100 µL of 0.1 M $NaHCO_3$ (freshly prepared).

Scale up mixture to have enough solution for the number of wells you have (40 µL each).

2. Mix thoroughly. Centrifuge solution to remove bubbles, 7200*g* for 1 minute.
3. Add 40µL of PEG mix solution to each well. Allow reaction for 2 hours**

Quantum dots:

1. Block surface
    a. 1% BSA for 1 hour
2. Prepare dilution of SA-QDots in blocking buffer such as 1% BSA.
3. Add 50 µL of QD solution to wells and leave for 15 minutes.
4. Wash 3 times with 1x borate buffer, leave wells filled with borate buffer for imaging. Be carefµL with pipette tip as it can scratch the surface and wipe away bound QDots.

2: Biotin-PEG-Silane surface prep for Streptavidin-conjugated Quantum Dots in Matrical 384-well glass-bottom plates.

Cleaning: Wells hold max ~120µL, use 100µL of each cleaning reagent. Use multichannel pipette to fill wells with each reagent, mix and remove. For KOH treatment use 40 µL to prevent creation of reactive sites up well walls.

1. Water (ultra-pure – MilliQ or Sigma)
2. 5% Alconox. Rinse 3 times with water to remove soap bubbles.
3. Isopropanol. Rinse with water after.
4. 1M KOH – let sit for 10 minutes. Rinse with water after.
5. Water

PEG-Silanization: Biotin-PEG-Silane MW 3400 and mPEG-Silane MW 2000. Biotin surface use Bio-PEG-Sil only, blank surface use mPEG-Sil only.

1. Remove water from wells and rinse/replace with methanol.
2. Clean glassware and rinse with methanol. Be sure to remove all water from glassware and wells.
3. Prepare a 1% silane mixture with: (or scale up volumes if needed)
    a. 25 mL methanol
    b. 1.25 mL acetic acid
    c. 25 mg BIO-PEG-SIL or 15 mg mPEG-SIL
4. Mix silanization solution well in a beaker and immediately add 100 µL each to wells.
5. Allow to react for 2 hours.
6. Remove reaction solution and rinse with methanol.
7. Wells can be rinsed and filled with ultrapure water and stored overnight at $4^{o}C$

Quantum dots:

1. Block surface: 100 µL BSA (1% in 1xPBS) for 1 hour.
2. Prepare dilutions of SA-QDots in blocking buffer (1% BSA) (1 pM to 1 fM dilution range)
3. Add 100 µL of QD solution to wells and leave for 30 min.
4. Wash 3 times with 1x PBS buffer, leave wells filled with buffer for imaging. Be careful with pipette tip as it can scratch the surface and wipe away bound QDots.

Notes:

- Similar procedure can be used with other manufacturer's multiwell glass-bottom plates, just ensure to use proper volume needed to cover the bottom surface of the wells (larger than 40 µL maybe needed).
- Be careful with multichannel pipet tips, as scratches in glass surface will cause irregularities in surface functionalization and QD aggregation.

3: Thiolated DNA on Maleimide-PEG surfaces in Matrical 384-well glass-bottom plates.

Cleaning: Wells hold max ~120µL, use 100µL of each cleaning reagent. Use multichannel pipette to fill wells with each reagent, mix and remove. For KOH treatment use 40 µL to prevent creation of reactive sites up well walls.

1. Water (ultra-pure – MilliQ or Sigma)
2. 5% Alconox. Rinse 3 times with water to remove soap bubbles.
3. Isopropanol. Rinse with water after.
4. 1M KOH – let sit for 10 minutes. Rinse with water after.
5. Water

Silanization: APTES or similar silane (e.g. N-(2-aminoethyl)-3-aminopropyltrimethoxysilane, 2-AE-APTMS).

1. Remove water from wells and rinse/refill with methanol.
2. Clean glassware and rinse with methanol. Be sure to remove all water from glassware and wells.
3. Prepare a 1% silane mixture with: (or scale up volumes if needed)
    a. 25 mL methanol
    b. 1.25 mL acetic acid
    c. 0.25 mL 2-AE-APTMS (or other silane)
4. Mix silane solution well in a beaker and immediately add to wells 50 µL to minimize creation of reactive sites up well walls).
5. Allow to react for 20 minutes.
6. Remove reaction solution and rinse/refill with methanol.

PEGylation: (SVA has a short hydrolysis half-life in aqueous solution (<30 min) so prepare the solution and use immediately). For mPEG-SVA (MW 2000) and MAL-PEG-SVA (MW 3400) in 20:1 molecular ratio:

1. 20:1 ratio of mPEG-SVA:MAL-PEG-SVA. Concentration used is:
    a. 5.0mg mPEG-SVA MW 2000
    b. 0.42mg MAL-PEG-SVA MW 3400
    c. Per 100 µL of 0.1 M $NaHCO_3$ (freshly prepared).
        i. Scale up recipe to have enough solution for the number of wells you have (50 µL each).
        ii. Weigh out two batches of PEG mix, to have a second reaction.
        iii. Also prepare for blank surfaces, solutions that are only mPEG (5.0 mg/100 µL)
2. Mix thoroughly. If needed, centrifuge solution to remove bubbles, 7200*g* for 1 minute.
3. (Remove methanol from wells and rinse well with water)
4. Add 50µL of PEG mix solution to each well. Allow reaction for 1 hour.
5. After first hour of reaction, remove solution and add another set of freshly prepared reaction mixture to wells. This second aliquot of PEG solids can be measured out prior and stored in desiccator then dissolved fresh.
6. Allow second reaction for 1 hour.

7. After reaction, wash wells with ultrapure water. Do not store for long periods of time; prepare thiol-DNA to be added immediately after this reaction is complete.

DNA Thioether reduction and clean up: Tris(2-carboxyethyl)phosphine hydrochloride (TCEP) to cleave thiol-linked protecting group from DNA-SH.
(*takes ~1 hour: start this when you start the second hour of PEG reaction to save waiting time)

1. Column hydration:
    a. Add 650 µL Sigma water to a Centrispin 10 column.
    b. Vortex for 15 s to remove air bubbles and let sit for 30 min.
2. Disulfide Cleavage and Reaction Clean up:
    a. [Make a fresh 50 mM solution of TCEP (15mg TCEP•HCl in 1 mL of 1x PBS).]
    b. Add 50 µL of 50 mM TCEP•HCl and 50 µL of 100 µM thiolated DNA to microcentrifuge tube and let sit for 30 min at RT.
    c. Remove spin column caps and put into flat bottom wash tubes (notches out)
    d. Centrifuge at 750*g* for 2 min to remove water
    e. Discard wash microcentrifuge tubes and place spin column in clean microcentrifuge tube with caps in.
    f. Apply DNA/TCEP•HCl reaction product solution to column and spin at 750*g* for 2 min (2.8 krpm). Cleaved DNA will be in the microcentrifuge tube.
    g. Determine the DNA concentration using a UV-Vis (Nanodrop) at 260 nm. Check the absorption coefficient in the IDT sheet.
        i. GAPDH cPRB-S is MW 7415 g/mol.
        ii. Nanodrop reports concentration in ng/µL. To convert ng/µL to µMolar:

$$\frac{[x]\,ng}{\mu L} * \frac{mol}{7415g} * \frac{1000\,\mu L * g}{ng * L} = \frac{[\,]\,\mu mol}{L}$$

3. Thiol Reaction on Maleimide functionalized Surfaces:
    a. Dilute the DNA-SH solution to 3µM in 1x PBS.
    b. Add 50µL of 3µM DNA-SH capture probe in a well and let react for 2h at room temp.
4. Wash wells with 1xPBS and can store overnight at 4$^{o}$C.

For calibration experiments, use concentration range 10 pM, 1 pM, 100 fM, 10 fM, 1 fM DNA. For testing parameters, only a few need to be prepared.

(A): Direct Hybridization with DNA-Biotin:

1. Prepare serial dilutions of biotinylated DNA anti-complement probes (GAPDH acPRB-BIO, or acPRB-dBIO for dual-biotinylated), in the hybridization buffer (4xPBS).
2. Add 100 µL of DNA-BIO to each well, allow hybridization for 4 hours on shaker at 200 RPM at room temp, covered.

3. Stringency washes: *[when washing, don't allow wells to completely empty and expose surface to dry air – instead adjust pipetting to remove/add enough that you always keep about 10 µL in the wells when you remove wash buffer.]
    a. Wash with hybridization buffer
    b. Wash 3x with stringency wash (#1)
    c. Wash 3x with general wash (#2)
4. Block surface with BSA 1% in 1xPBS (= 10 mg/mL) for 1 hour
5. Add 50 µL 0.5pM streptavidin-QDots diluted in 1%BSA/1xPBS for 30 min
6. Wash with 1x PBS buffer and leave >50 µL of buffer in wells for imaging – *Don't let well surface dry

(B): DNA Sandwich Assay:

1. Prepare serial dilutions of target DNA (GAPDH Sand-Target), in the hybridization buffer (4xPBS) at various concentrations (1 pM to 1 fM).
2. Add 100 µL of tDNA to each well, allow hybridization for (4 to 12 hours)* at room temp, covered.
3. Stringency washes: *[when washing, don't allow wells to completely empty and expose surface to dry air – instead adjust pipetting to remove/add enough that you always keep about 10 µL in the wells when you remove wash buffer.]
    a. Wash with hybridization buffer
    b. Wash 3x with stringency wash (#1)
    c. Wash 3x with general wash (#2)
4. Prepare signal probe DNA (GAPDH sPRB-dbiot or sPRB-biot), in the hybridization buffer (4xPBS) at (5 pM to 50 pM)*.
5. Add 100 µL of DNA-BIO to each well, allow hybridization for 4 hours at room temp, covered.
6. Stringency washes:
    a. Wash with hybridization buffer
    b. Wash 3x with low stringency wash (#1)
    c. Wash 3x with high stringency wash (#2)
7. Block surface with BSA 1% in 1xPBS (= 10 mg/mL) for 1 hour
8. Add 50 µL 0.5pM streptavidin-QDots diluted in 1%BSA/1xPBS for 30 min
9. Wash with 1x PBS buffer and leave >50 µL of buffer in wells for imaging – *Don't let well surface dry

Solution preparation:

- Hybridization buffer: 4x PBS (4 mL of 10xPBS buffer, 6 mL water)
- Low Stringency Wash: 0.2% SDS, 2x SSC (400 µL 20% SDS, 4 mL 20x SSC, 35.6 mL water)
- High Stringency Wash : 0.05x SSC (100 µL 20xSSC 39.9 mL water)

## Appendix 2: ImageJ Macro for QD Counting

Macro file: “Particle_count_tiff_-_MML_MJD.txt”

The macro can be installed and used by running ImageJ, and clicking Plugins>Macros>Install… and then navigating to the macro text file and selecting it. The button will appear in the ImageJ toolbar as a black square with white dots. Alternately the macro can be run once by clicking Plugins>Macros>Run… and selecting the text file.

Lines:

22-40: Assigns default parameters.

42-76: Dialog box for improved user interface and ability to change parameters. Credit to Mitchell Duffy, Tufts 2012, for writing this section.

77-100: Constructs data tables for output.

103: Start of main program.

105-133: File management, gets list of CXD files in the user’s chosen directory, opens each file and converts to a 16-bit multi-page TIFF movie file. Saves each new TIFF file and deletes the CXD files. This block is executed only if the user has specified that the starting files are in CXD format. Utilizes the LOCI Bio-Formats Importer plugin, freely available online from http://loci.wisc.edu/software/bio-formats, ©University of Wisconsin-Madison. These functions could be modified to use to any other non-standard microscope file type.

135-onwards uses TIFF files.

136-140: Gets list of all TIFF movie files that exist in the directory.

142-242: All image processing and threshold & particle count analysis is done here for each TIFF file now in the directory. Each of these instructions is executed on each individual file:

143-157: Processing filename and opening the stack

162-167: Creates two projections, the SUM and STD. Converts each to the same 8-bit scale.

170-172: Uses the “Merge Channels” tool to create a composite image, converts to 8-bit grayscale and saves this file as the image name appended with “_RGB”.

174-176: Uses the “Convolve” tool.

177-178: Retrieves some basic statistics about the image histogram. Note: do not confuse this average ('mean') and standard deviation ('std') with the projection methods AVG, SUM, or STD. These statistics refer to the set of pixels in the current single image.

179-187: Chooses the number of threshold steps to take, depending on the image statistics. The standard deviation of all pixel values in this single image is used as a value indicative of high noise level; if the std value is higher than the specified cut-off then a wider range of threshold is sampled to avoid this high background.

191-199: Uses "Threshold" and "Analyze Particles" tools, looping over the range of threshold steps as fractions (0.03 to 0.255 or to 0.53) of the image intensity range (0 to 255). Creates a of particle counts taken at each threshold step.

208-228: Calculates "assess" value for each space, stepping over each index in the array of counts, taking five values at a time and incrementing this five-space window over the whole array of counts. The "assess" value is defined as the absolute value of the difference between the *n*th space and the $(n+5)^{th}$ space, multiplied by the fraction (or the square of the fraction) that this *n*th index represents in the threshold steps. As the algorithm is looping and incrementing this threshold window it tracks the lowest "assess" value and stores the index of the 5-point range to that gives this optimum value.

The two methods here, difference*fraction and difference*fraction^2, can be selected by the user. They usually select similar or identical ranges, but using the difference*fraction comparison seems to give more consistent results in images with low particle count while difference*fraction^2 may be more error-prone in these low-count images but can perform betting in very dense, bright images.

224-232: Prints out selected optimum range. The original image title and the computed particle count are sent to the data table titled "Counts".

This ends the instructions executed for each TIFF file.

240-247: Data tables are saved as Excel spreadsheets to the user-specified "Output" directory.

260-273: Function to populate an array with the names of all CXD files in the directory. This function implements a depth-first, recursive method and takes each filename that ends in ".cxd" only.

275-288: Function to populate an array with the names of all TIFF stacks in the directory. This function implements a depth-first, recursive search and takes each filename that ends in ".tif" only, and ignores any TIFF files with the tags such as "SUM.tif" and "RGB.tif" which are added to files created during use of this program.

290-305: Function to extract some part of the filename. The filepath contains the full path, which is identical through the head directory. It removes these first segments of the filepath and returns only the last part of the filepath which contains the unique descriptor folder names. (i.e. "Z:\Mike\TIRF Data\TIRF data Feb 2 4 11 15\TIRF Data Feb 11\10 pM\" would be shortened to "10 pM\Data10.tif")

Macro file: “Particle_count_tiff_-_MML_MJD.txt” available on Tufts Walt Lab server share.

```
// Michael M. Lacy
// QD Counting Macro
// Written for Tufts University Chemistry, David Walt group 2010.

// Macro program for counting particles. The algorithm used is optimized for
// detecting quantum dots. The program uses the standard deviation projection
// which we have shown to improve QD detection.

// Begin by selecting the head folder containing all files and folders to search
// through and count. Sets increasing stepwise threshold and stepwise threshold
// and counts particles. Detects images with high background variation and takes
// more steps to avoid background in particle counting. Interrogates count vs.
// threshold data to find range of 5 steps with least relative variation, using
// method of finding minimum (value5-value1)*frac^2, this value is related to the
// derivative of the count vs. threshold curve, to find the optimum range approaching
// a plateau or peak, indicative of the accurate number of particles present.
//
// To convert from CXD images from microscope, the LOCI Bio-Formats importer is
// required, available online at loci.wisc.edu/software/bio-formats.
//

macro "Particle Count Action Tool - C000D00D01D02D03D04D05D06D07D08D09D0aD0bD0cD0dD0eD0fD10D11D12D13D14D15D16D18D19D1aD1bD1cD1dD1eD1fD20D21D

  outputLocation = "C:\\Documents and Settings\\mlacy01\\Desktop\\";            //will save data tables as excel spreadsheets to specified output location.

  nfiles = 800;
  setBatchMode(true);
  base = 0.03;
  oSteps = 45;                  // number of points thresholding will take.  will step from 0 to < (steps), and will choose:
  hSteps = 100;                 //here oSteps for original step number, will later choose a value for steps = either oSteps or hSteps.

  incr = 0.005;                 // increment, fraction of intensity range will be stepping by.
  cutOff = 7;                   //cut-off value for "high-background" (high-variation), marking image to use larger number of steps.
  frac = base;
  thrs = 0;
  sizeMin = 2;
  sizeMax = 12;

  applyConvolve = true;
  multType = "diff*frac";  //default advance options

  requires("1.34m");
  Dialog.create("Particle Count Options");
  Dialog.addNumber("Minimum Particle Size: ", sizeMin);
  Dialog.addNumber("Maximum Particle Size: ", sizeMax);
  Dialog.addString("Save Output Count File To: ", outputLocation, 50);
  Dialog.addCheckbox("Convert .CXD files to .TIF before processing? (Deletes original .cxd files!)", false);
  Dialog.addCheckbox("Browse for Output Location", false);
  Dialog.addCheckbox("Advanced Options", false);
  Dialog.show();
  sizeMin = Dialog.getNumber();
  sizeMax = Dialog.getNumber();
  outputLocation = Dialog.getString();
  isCxd = Dialog.getCheckbox();
  browse = Dialog.getCheckbox();
  advOptions = Dialog.getCheckbox();

  if (browse == true)
  {
    outputLocation = getDirectory("Choose a Directory for Output Data");
  }

  if (advOptions == true)
  {
```

```
65      Dialog.create("Advanced Options");
66      Dialog.addNumber("Starting Threshold Fraction: ", base);
67      Dialog.addNumber("Standard Deviation High Backgroungd Cutoff: ", cutOff);
68      Dialog.addCheckbox("Apply Convolver", true);
69      Dialog.addChoice("Threshold Assessment Method: ", newArray( "diff*frac^2", "diff*frac"));
70      Dialog.show();
71      base = Dialog.getNumber();
72      cutOff = Dialog.getNumber();
73      applyConvolve = Dialog.getCheckbox();
74      multType = Dialog.getChoice();
75    }
76
77    // data tables for output.
78    requires("1.41g");
79    title1 = "Particle Count Data";       // raw-data, table t
80    title2 = "["+title1+"]";
81    title3 = "Counts";                            // simple-output, table t2
82    title4 = "["+title3+"]";
83    t = title2;                                           // use t for printing to raw data table.
    and t2 for simple output table
84    t2 = title4;
85    if (isOpen(title1)){
86          if (getBoolean("Clear data table? No: keep data, Cancel: exit macro")){
87                print(t, "\\Clear");            //clears the window t.
88          }
89    }
90    else
91          run("Table...", "name=" + title2 + " width=700 height=700");
92    print(t, "\\Headings:Threshold\tParticle count\tThreshold fraction");
93    if (isOpen(title3)){
94          if (getBoolean("Clear data table? No: keep data, Cancel: exit macro")){
95                print(t2, "\\Clear");           //clears the window t.
96          }
97    }
98    else
99          run("Table...", "name=" + title4 + " width=500 height=500");
100   print(t2, "\\Headings:Image\tParticle count\tIndex");
101
102
103   // main program //
104
105   print("\\Clear");
106   dir = getDirectory("Choose a Directory for Input Data");
107   startTime = getTime();        // for measuring program performance
108
109   if(isCxd == true){
110     n = 0;
111     allfiles = newArray(nfiles);      //will put file names in array, but so many spaces so not
    likely ever to have too many files.
112
113     n = listFilesCXD(dir, allfiles, n);   //need to catch n, returns number of files found with CXD
    format.
114     if(n <= 0){
115       exit("There are no .cxd files in this folder.");
116     }
117     print(n + " CXD files located.");
118     filenames = Array.trim(allfiles, n);  //allfiles array has n useful filenames (index from 0)
    and rest is empty.
119     for(p = 0; p < n; p++){
120       print("\\Update1:Opening: " + (p+1) + ": " + filenames[p]);
121       run("Bio-Formats Importer", "open=[" + filenames[p] + "] autoscale color_mode=Default view=
    [Standard ImageJ] stack_order=Default"); //opens next target .cxd file with LOCI Bio-Formats plugin.
122       file = getTitle();
123       filenospc = replace(file, " ", "_");
124       fullnospc = replace(filenames[p], file, filenospc);     //will crash later if spaces in
    filename when going to projections
125       newtiff = substring(fullnospc, 0, (lengthOf(fullnospc) - 3)) + "tif"; //cut off cxd from file
    name, replace with tif - good to go.
126       print("\\Update2:Saving: " + newtiff);
127       saveAs("Tiff", newtiff);
```

```
128         File.delete(filenames[p]);
129         if (nImages() != 0){
130           close();        // close the active image window, or else will run out of active memory
    with all the images open.
131         }
132       }
133     }
134
135
136     n = 0;
137     allfiles = newArray(nfiles);      //will put file names in array, but so many spaces so not
    likely ever to have too many files.
138
139     n = listFilesTIFF(dir, allfiles, n);          // analogous to listFilesCXD()...
140     print(n + " files located.");
141     filenames = Array.trim(allfiles, n);
142     for(p = 0; p < n; p++){
143           print("\\Update1:" + filenames[p]);             //print current filename.
144           print("\\Update2:File " + (p+1) + " of " + n);  //updates Log window with progress
145           open(filenames[p]);
146           if (p == 0){   //converted full batches, so should only need to check once.
147                   if(bitDepth != 16){             //if not 16 bit format, exit macro.
148                           exit("The image is not 16-bits!");
149                   }
150           }
151           stack = getTitle();                     // name of window for original stack, is not full
    filename.
152
153           stacknospc = replace(stack, " ", "");
154           filenospc = replace(filenames[p], stack, stacknospc);
155           File.rename(filenames[p], filenospc);
156           stack = stacknospc;
157           rename(stack);
158
159           print(t, "");
160           print(t, filenames[p]);         // full filename.
161           slices = nSlices;
162           project = newArray("Standard Deviation", "Sum Slices"); //which projection(s) to be used.
163           for(z = 0; z < 2; z++){         // loop through three z-project types
164                   selectWindow(stack);
165                   run("Z Project...", "start=1 stop=slices projection=[" + project[z] + "]");
166                   run("8-bit");
167           }
168           selectWindow(stack);
169           close();                                                          // close original stack
    image, left with three projections.
170           run("Merge Channels...", "red=SUM_" + stack + " green=*None*" + " blue=STD_" + stack + "
    gray=*None*");  //also closes images
171           run("8-bit");
172           save(substring(filenospc, 0, (lengthOf(filenospc) - 4)) + "_RGB.tif");          //replace
    ".tif" with "_RGB.tif" for new filename for RGB composite.
173           activeImg = getTitle;
174           if(applyConvolve == true){
175             run("Convolve...", "text1=[-1 -1 -1\n-1 8  -1\n-1 -1 -1\n] normalize");
176       }
177           getStatistics(area, mean, min, max, std, histogram);    //retrieve image statistics
178           range = max - min;
179           if(std >= cutOff){  // high std of image indicates higher levels of background, so take
180                                                   // more steps to pass the low thresholds where
    background will interfere.
181                   steps = hSteps;
182                   countsArray = newArray(steps);
183       }
184           if(std < cutOff){
185                   steps = oSteps;
186                   countsArray = newArray(steps);
187           }
188           print(t, "Image name\tStd\tMax Pixel");
189           print(t, activeImg + "\t" + std + "\t" + max);
190           print(t, "Threshold\tCount\tFraction");
```

```
191         for(f = 0; f < steps; f++){             // Use image min&max to calculate threshold values
    from fractions,
192                 frac = base + (f*incr);                 // set thresholds and count particles and
    put the results into the data table.
193                 thrs = min + range*frac;
194                 run("Threshold...");
195                 setThreshold(thrs, max);
196                 run("Analyze Particles...", "size=" + sizeMin + "-" + sizeMax + "
    circularity=0.00-1.00 show=Nothing clear");
197                 countsArray[f] = nResults;                      // put number of particles counted
    into array, index is the step number, so can work backwards from that too
198                 print(t, thrs + "\t" + countsArray[f] + "\t" + frac);
199         }                       //end loop for f, setting thresholds, counting, printing to table.
200                                 //now to find the 'best range':
201         minRange = 0;                   //index of the first step in a range of 5 values that has
    the lowest difference.
202         assess = 0;                         //assessment value
203         minSum = 1000;                  //arbitrary.  just need to start high then go and find
    minimum being less than this.
204         bestRangeAvg = 0;
205         ra1 = newArray(5);              //array to fill, cycling through each subset of 5 values in
    the data.
206         print(t, "");
207         print(t, "i\tassessment value");
208         for(s = 0; s < (steps-5); s++){         //interrogating each set of 5 values, incrementing
    the start of the set by one step each time
209                 for(pt = 0; pt < 5; pt++){
210                         ra1[pt] = countsArray[s + pt];
211                 }
212                 Array.getStatistics(ra1, min, max, mean, stdDev);
213                                         //two possible assessment methods diff*frac or diff*frac^2
214       if(multType == "diff*frac"){
215                 assess = abs(ra1[0] - ra1[4])*(base + (s + 2.5)*incr);  // =diff*frac^2, as frac is
    centered for the range.
216       }
217       else if(multType == "diff*frac^2"){
218                 assess = abs(ra1[0] - ra1[4])*(base + (s + 2.5)*incr)*(base + (s + 2.5)*incr);
219       }
220       else{ exit("Invalid Multiplication Type!"); }
221
222                 if(assess < minSum){      //interrogating to find the minimum: its value and index.
223                         minSum = assess;          //if a new lowest value, store/set this as the
    new min.
224                         minRange = s;
225                         bestRangeAvg = mean;  //meanof this range, store as new lowest val to
    compare to.
226                 }                               //minRange now equals the index of the first step
    for the 'best' range of 5 counts.
227                 print(t, s + "\t" + assess);
228         }                       //end loop s
229
230         print(t, "");
231         print(t, "best range attempt:\tCount");
232         for(i = 0; i < 5; i++){
233                 print(t, (minRange+i) + "\t" + countsArray[(minRange+i)]);
234         }
235         print(t, "average in range");
236         print(t, bestRangeAvg);
237         folderSet = descriptionFolders(filenames[p]);
238         print(t2, folderSet + "\t" + bestRangeAvg + "\t" + minRange);
239         if (nImages() != 0){
240                 close();                                // closes the active image window
241         }
242   }     //end loop for p, filenames
243
244   print("\\Clear");
245   print(n + " Files complete.");
246   MonthNames = newArray("Jan","Feb","Mar","Apr","May","Jun","Jul","Aug","Sep","Oct","Nov","Dec");
247   getDateAndTime(year, month, dayOfWeek, dayOfMonth, hour, minute, second, msec);
248   titleStr1 = title1 + " " + MonthNames[month] + " " + dayOfMonth;
```

```
  selectWindow(title1);
  saveAs("Text", outputLocation + titleStr1 + ".xls");                  //save Particle count data table
  titleStr2 = title3 + " " + MonthNames[month] + " " + dayOfMonth;
  selectWindow(title3);
  saveAs("Text", outputLocation + titleStr2 + ".xls");                  //save Counts output
  endTime = getTime();
  timeElapsed = endTime - startTime;
  minElapsed = timeElapsed/60000;
  print("Program took " + minElapsed + " minutes.");

}

  //end of macro


//functions:

function listFilesCXD(dir, bigList, n) {
  list = getFileList(dir);            //file names within the dir.
  for(i=0; i < list.length; i++){
    if(endsWith(list[i], "/")){         // if ends in "/" its a folder, so
      list[i] = "" + substring(list[i], 0, (lengthOf(list[i]) - 1)) + "\\";   //append it with backslash to make coherent file path.
      n = listFilesCXD(""+dir+list[i], bigList, n);         // fcn calls itself, to go thru that folder. (""+dir+list[i]) is a string, now is the new arg to go into that folder.
    }
    if(endsWith(list[i], ".cxd")){        //for each .cxd file only,
      bigList[n] = dir + list[i];       //assign filename to next index in the bigList array
      n = n+1;              //increment n.
    }
  }
    return n;
}//end of function listFilesCXD

function listFilesTIFF(dir, bigList, n) {
        list = getFileList(dir);                                        //file names within the dir.
        for(i=0; i < list.length; i++){
                if(endsWith(list[i], "/")){                                             // if ends in "/" its a folder, so
                        list[i] = "" + substring(list[i], 0, (lengthOf(list[i]) - 1)) + "\";             //append it with backslash to make coherent file path.
                        n = listFilesTIFF(""+dir+list[i], bigList, n);                  // fcn calls itself, to go thru that folder. (""+dir+list[i]) is a string, now is the new arg to go into that folder.
                }
                if((endsWith(list[i], ".tif") == true) && ((endsWith(list[i], "RGB.tif")|endsWith(list[i], "SUM.tif")|endsWith(list[i], "AVG.tif") == false))){          //for each .tif file only, but not RGB files created previously. can re-reun macro and need not delete
                        bigList[n] = dir + list[i];                     //assign filename to next index in the bigList array
                        n = n+1;                                                //increment n.
                }
        }
        return n;
}               //end of function listFiles

function descriptionFolders(filename){
        sl = newArray(lengthOf(filename));
        in = 0;
        slashes = newArray(lengthOf(filename));
        for(q = 0; q < (lengthOf(filename) - 1); q++){
                sl[q] = indexOf(filename, "\\", (q+1));
                if(sl[q] > 0){
                        slashes[in++] = (sl[q]);
                        q = sl[q];
                }
                if(sl[q] < 0){
                        q = lengthOf(filename);
                }
        }
        return substring(filename, slashes[3] + 1);
}               //end of function descriptionFolders
```

## References


1. Rissin, D. M.; Gorris, H. H.; Walt, D. R. Distinct and long-lived activity states of single enzyme molecules. *Journal of the American Chemical Society* **2008**, *130*, 5349-53.
2. Wayment, J. R.; Harris, J. M. Biotin-avidin binding kinetics measured by single-molecule imaging. *Analytical Chemistry* **2009**, *81*, 336-42.
3. Bishop, J.; Chagovetz, a M.; Blair, S. Kinetics of multiplex hybridization: mechanisms and implications. *Biophysical Journal* **2008**, *94*, 1726-34.
4. Temirov, J. P.; Bradbury, A. R. M.; Werner, J. H. Measuring an antibody affinity distribution molecule by molecule. *Analytical Chemistry* **2008**, *80*, 8642-8.
5. Warshaw, D. M.; Kennedy, G. G.; Work, S. S.; Krementsova, E. B.; Beck, S.; Trybus, K. M. Differential labeling of myosin V heads with quantum dots allows direct visualization of hand-over-hand processivity. *Biophysical Journal* **2005**, *88*, L30-2.
6. van Oijen, A. M. Single-molecule approaches to characterizing kinetics of biomolecular interactions. *Current opinion in biotechnology* **2011**, *22*, 75-80.
7. Taniguchi, Y.; Choi, P. J.; Li, G.-W.; Chen, H.; Babu, M.; Hearn, J.; Emili, A.; Xie, X. S. Quantifying E. coli Proteome and Transcriptome with Single-Molecule Sensitivity in Single Cells. *Science* **2010**, *329*, 533-538.
8. Diehl, F.; Diaz, L. A. Digital quantification of mutant DNA in cancer patients. *Current Opinion in Oncology* **2007**, *19*, 36-42.
9. Saiki, R. K.; Scharf, S.; Faloona, F.; Mullis, K. B.; Horn, G. T.; Erlich, H. A; Arnheim, N. Enzymatic amplification of beta-globin genomic sequences and restriction site analysis for diagnosis of sickle cell anemia. *Science* **1985**, *230*, 1350-1354.
10. Engvall, E.; Perlmann, P. Enzyme-linked immunosorbent assay (ELISA). Quantitative assay of immunoglobulin G. *Immunochemistry* **1971**, *8*, 871-4.
11. Zhang, H.; Zhao, Q.; Li, X.-F.; Le, X. C. Ultrasensitive assays for proteins. *The Analyst* **2007**, *132*, 724-37.
12. Lipson, D.; Raz, T.; Kieu, A.; Jones, D. R.; Giladi, E.; Thayer, E.; Thompson, J. F.; Letovsky, S.; Milos, P.; Causey, M. Quantification of the yeast transcriptome by single-molecule sequencing. *Nature Biotechnology* **2009**, *27*, 652-8.
13. Eid, J.; Fehr, A.; Gray, J.; Luong, K.; Lyle, J.; Otto, G.; Peluso, P.; Rank, D.; Baybayan, P.; Bettman, B.; Bibillo, A.; Bjornson, K.; Chaudhuri, B.; Christians, F.; Cicero, R.; Clark, S.; Dalal, R.; Dixon, J.; Foquet, M.; Gaertner, A.; Hardenbol, P.; Heiner, C.; Hester, K.; Holden, D.; Kearns, G.; Kong, X.; Kuse, R.; Lacroix, Y.; Lin, S.; Lundquist, P.; Ma, C.; Marks, P.; Maxham, M.; Murphy, D.; Park, I.; Pham, T.; Phillips, M.; Roy, J.; Sebra, R.; Shen, G.; Sorenson, J.; Tomaney, A.; Travers, K.; Trulson, M.; Vieceli, J.; Wegener, J.; Wu, D.; Yang, A.; Zaccarin, D.; Zhao, P.; Zhong, F.; Korlach, J.; Turner, S. Real-Time DNA Sequencing from Single Polymerase Molecules. *Science* **2009**, *323*, 133-138.

14. Rissin, D. M.; Kan, C. W.; Campbell, T. G.; Howes, S. C.; Fournier, D. R.; Song, L.; Piech, T.; Patel, P. P.; Chang, L.; Rivnak, A. J.; Ferrell, E. P.; Randall, J. D.; Provuncher, G. K.; Walt, D. R.; Duffy, D. C. Single-molecule enzyme-linked immunosorbent assay detects serum proteins at subfemtomolar concentrations. *Nature Biotechnology* **2010**, *28*, 595-9.

15. Cornish, P.; Ha, T. A Survery of single-molecule techniques in chemical biology. *ACS Chemical Biology* **2006**, *2*, 53-61.

16. Fries, J. R.; Brand, L.; Eggeling, C.; Köllner, M.; Seidel, C. A. M. Quantitative Identification of Different Single Molecules by Selective Time-Resolved Confocal Fluorescence Spectroscopy. *The Journal of Physical Chemistry A* **1998**, *102*, 6601-6613.

17. Jarvius, J.; Melin, J.; Goransson, J.; Stenberg, J.; Fredriksson, S.; Gonzalez-Rey, C.; Bertilsson, S.; Nilsson, M. Digital quantification using amplified single- molecule detection. *Nature Methods* **2006**, *3*, 725-727.

18. Göransson, J.; Wählby, C.; Isaksson, M.; Howell, W. M.; Jarvius, J.; Nilsson, M. A single molecule array for digital targeted molecular analyses. *Nucleic Acids Research* **2009**, *37*.

19. Tessler, L. A; Reifenberger, J. G.; Mitra, R. D. Protein quantification in complex mixtures by solid phase single-molecule counting. *Analytical Chemistry* **2009**, *81*, 7141-8.

20. Simon, S. M. Partial internal reflections on total internal reflection fluorescent microscopy. *Trends in Cell Biology* **2009**, *19*, 661-8.

21. Axelrod, D. Cell-substrate contacts illuminated by total internal reflection fluorescence. *The Journal of Cell Biology* **1981**, *89*, 141-5.

22. Trache, A.; Meininger, G. Total internal reflection fluorescence (TIRF) microscopy. In *Current Protocols in Microbiology* **2008**, *Chapter 2*.

23. Chan, H.-M.; Chan, L.-S.; Wong, R. N.-S.; Li, H.-W. Direct quantification of single-molecules of microRNA by total internal reflection fluorescence microscopy. *Analytical Chemistry* **2010**, *82*, 6911-8.

24. Wang, J.; Fu, G.; Wang, C.; Liu, L.; Wang, G. Single dye molecules observed by total internal reflection fluorescence microscopy. *Proceedings of SPIE* **2007**, *6534*, 65341B-65341B-6.

25. Kobitski, A.; Heyes, C.; Nienhaus, G. Total internal reflection fluorescence microscopy: A powerful tool to study single quantum dots. *Applied Surface Science* **2004**, *234*, 86-92.

26. Zhao, R.; Rueda, D. RNA folding dynamics by single-molecule fluorescence resonance energy transfer. *Methods* **2009**, *49*, 112-7.

27. Xiao, M.; Phong, A.; Ha, C.; Chan, T.-F.; Cai, D.; Leung, L.; Wan, E.; Kistler, A. L.; DeRisi, J. L.; Selvin, P. R.; Kwok, P.-Y. Rapid DNA mapping by fluorescent single molecule detection. *Nucleic Acids Research* **2007**, *35*, e16.

28. Crut, A.; Géron-Landre, B.; Bonnet, I.; Bonneau, S.; Desbiolles, P.; Escudé, C. Detection of single DNA molecules by multicolor quantum-dot end-labeling. *Nucleic Acids Research* **2005**, *33*.

29. Li, L.; Li, X.; Li, L.; Wang, J.; Jin, W. Ultra-sensitive DNA assay based on single-molecule detection coupled with fluorescent quantum dot-labeling and its application to determination of messenger RNA. *Analytica Chimica Acta* **2010**, *685*, 52-7.

30. Sui, B.; Li, L.; Li, L.; Jin, W. An ultra-sensitive DNA assay based on single-molecule detection coupled with hybridization accumulation and its application. *The Analyst* **2011**, 6-11.

31. Jain, A.; Liu, R.; Ramani, B.; Arauz, E.; Ishitsuka, Y.; Ragunathan, K.; Park, J.; Chen, J.; Xiang, Y. K.; Ha, T. Probing cellular protein complexes using single-molecule pull-down. *Nature* **2011**, *473*, 484-488.

32. Alivisatos, A. P. Semiconductor Clusters, Nanocrystals, and Quantum Dots. *Science* **1996**, *271*, 933-937.

33. Bruchez Jr., M.; Moronne, M.; Gin, P.; Weiss, S.; Alivisatos, A. P. Semiconductor Nanocrystals as Fluorescent Biological Labels. *Science* **1998**, *281*, 2013-2016.

34. Chan, W. C.; Nie, S. Quantum Dot Bioconjugates for Ultrasensitive Nonisotopic Detection. *Science* **1998**, *281*, 2016-2018.

35. "The Future of Fluorescence: Qdot nanocrystal technology". Invitrogen Corp. **2008**.

36. Bentolila, L. A.; Michalet, X.; Weiss, S. Quantum Optics: Colloidal Fluorescent Semiconductor Nanocrystals (Quantum Dots) in Single-Molecule Detection and Imaging. In *Single Molecules and Nanotechnology*; Rigler, R.; Vogel, H., Eds.; Springer-Verlag: Berlin Heidelberg, **2008**; pp. 53-81.

37. Resch-Genger, U.; Grabolle, M.; Cavaliere-Iaricot, S.; Nitschke, R.; Nann, T. Quantum dots versus organic dyes as fluorescent labels. *Nature Methods* **2008**, *5*, 763-775.

38. Nirmal, M.; Dabbousi, B. O.; Bawendi, M. G.; Macklin, J. J.; Trautman, J. K.; Harris, T. D.; Brus, L. E. Fluorescence Intermittency in Single Cadmium Selenide Nanocrystals. *Nature* **1996**, *383*, 802-804.

39. Broder, G. R.; Ranasinghe, R. T.; Neylon, C.; Morgan, H.; Roach, P. L. Kinetics and thermodynamics of biotinylated oligonucleotide probe binding to particle-immobilized avidin and implications for multiplexing applications. *Analytical Chemistry* **2011**, *83*, 2005-11.

40. Yang, Z.; Galloway, J. A.; Yu, H. Protein Interactions with Poly(ethylene glycol) Self-Assembled Monolayers on Glass Substrates: Diffusion and Adsorption. *Langmuir* **1999**, *15*, 8405-8411.

41. Roy, R.; Hohng, S.; Ha, T. A practical guide to single-molecule FRET. *Nature Methods* **2008**, *5*, 507-516.

42. Ha, T.; Selvin, P. R.; Joo, C. Single-molecule FRET with Total Internal Reflection Microscopy. In *Single Molecule Techniques*; Cold Spring Harbor Laboratory Press, **2008**; pp. 1-36.

43. Langmuir, I. The Adsorption of Gases on Plane Surfaces of Glass, Mica and Platinum. *Journal of the American Chemical Society* **1918**, *345*, 1361-1403.

44. Jokerst, J. V.; Lobovkina, T.; Zare, R. N.; Gambhir, S. S. Nanoparticle PEGylation for imaging and therapy. *Nanomedicine* **2011**, *6*, 715-28.

45. Kuno, M.; Fromm, D. P.; Hamann, H. F.; Gallagher, A.; Nesbitt, D. J. Nonexponential "blinking" kinetics of single CdSe quantum dots: A universal power law behavior. *The Journal of Chemical Physics* **2000**, *112*, 3117.

46. Bharadwaj, P.; Novotny, L. Robustness of quantum dot power-law blinking. *Nano Letters* **2011**, *11*, 2137-41.

47. Bentolila, L. A.; Weiss, S. Single-step multicolor fluorescence in situ hybridization using semiconductor quantum dot-DNA conjugates. *Cell Biochemistry and Biophysics* **2006**, *45*, 59-70.

48. Chen, Y.; Vela, J.; Htoon, H.; Casson, J. L.; Werder, D. J.; Bussian, D.A.; Klimov, V. I.; Hollingsworth, J. A. "Giant" multishell CdSe nanocrystal quantum dots with suppressed blinking. *Journal of the American Chemical Society* **2008**, *130*, 5026-7.

49. Mahler, B.; Spinicelli, P.; Buil, S.; Quelin, X.; Hermier, J.-P.; Dubertret, B. Towards non-blinking colloidal quantum dots. *Nature Materials* **2008**, *7*, 659-64.

50. Vela, J.; Htoon, H.; Chen, Y.; Park, Y.-S.; Ghosh, Y.; Goodwin, P. M.; Werner, J. H.; Wells, N. P.; Casson, J. L.; Hollingsworth, J. A. Effect of shell thickness and composition on blinking suppression and the blinking mechanism in "giant" CdSe/CdS nanocrystal quantum dots. *Journal of Biophotonics* **2010**, *3*, 706-17.

51. Wang, X.; Ren, X.; Kahen, K.; Hahn, M. a; Rajeswaran, M.; Maccagnano-Zacher, S.; Silcox, J.; Cragg, G. E.; Efros, A. L.; Krauss, T. D. Non-blinking semiconductor nanocrystals. *Nature* **2009**, *459*, 686-9.

52. Hohng, S.; Ha, T. Near-complete suppression of quantum dot blinking in ambient conditions. *Journal of the American Chemical Society* **2004**, *126*, 1324-5.

53. Antelman, J.; Ebenstein, Y.; Dertinger, T.; Michalet, X.; Weiss, S. Suppression of quantum dot blinking in DTT-doped polymer films. *The Journal of Physical Chemistry C, Nanomaterials and Interfaces* **2009**, *113*, 11541-11545.

54. Chen, Y.; Nguyen, A.; Niu, L.; Corn, R. M. Fabrication of DNA microarrays with poly(L-glutamic acid) monolayers on gold substrates for SPR imaging measurements. *Langmuir* **2009**, *25*, 5054-60.

55. Parak, W. J.; Gerion, D.; Zanchet, D.; Woerz, A. S.; Pellegrino, T.; Micheel, C.; Williams, S. C.; Seitz, M.; Bruehl, R. E.; Bryant, Z.; Bustamante, C.; Bertozzi, C. R.; Alivisatos, A. P. Conjugation of DNA to Silanized Colloidal Semiconductor Nanocrystalline Quantum Dots. *Chem. Mater.* **2002**, 2113-2119.

56. Gunnarsson, A.; Jönsson, P.; Zhdanov, V. P.; Höök, F. Kinetic and thermodynamic characterization of single-mismatch discrimination using single-molecule imaging. *Nucleic Acids Research* **2009**, *37*, e99.

57. "Methoxy poly(ethylene glycol) succinimidyl valerate (mPEG-SVA)". Laysan Bio Inc. Accessed online May **2011**.